Abstract

Contents

Chapter 1

Introduction

1.1 Overview

Fluid motions driven by buoyancy and frictional forces belongs to broad class of flows known as thermoconvective shear flows. These flows exhibit rich behaviour, and are of interest in both engineering and meteorology applications spanning across a broad range of length scales. At small scales, around $L \sim 1cm$, the thermoconvection flows are relevant to the cooling of microprocessing chips. In such systems, the fluid acts medium to dissipate heat, experiences shear forces from the confining walls, and buoyancy from heating. One of the major innovation in this industry is in squeezing more transistors onto a single chip, resulting to a doubling of transistors on a single chip roughly every two years, according to Moore's law. However, one of the major limitations on further miniaturisation is the challenge of dissipating the excessive heat generated. Fluids, such as air, water or refrigerant, are often used to transport heat away from the components, thereby preventing overheating [Kennedy and Zebib, 1983, Ray and Srinivasan, 1992]. At intermediate length scales, $L \sim 1m$, the interaction between buoyancy and frictional forces is important in the fabrication of uniform thin films in chemical vapour deposition (CVD) [Evans and Greif, 1991, Jensen et al., 1991]. The CVD process typically involves a reactive gases carried by inert gases which flows through a channel with a heated substrate. Upon heating, the reactant gases react chemically at substrate and deposits material, forming thin films, such as silicon layers. A key challenge in the CVD process is achieving a uniform deposition and maintaining sharp interfaces between layers. The interactions between shear and buoyancy forces often gives rise to boundary layers and thermoconvective rolls, which can disrupt uniform deposition, affecting fillm quality. At large scales, $L \sim 1km$, the thermoconvective shear flows can be observed in the atmosphere such as the cloud streets over the Norwegian Sea. These parallel bands of cumulus clouds can stretch over hundreds of kilometres. They form when relatively warm sea surfaces heat up the colder air blowing from the North [nor]. As the colder air is heated, it rises upwards whilst carrying water vapour. As it reaches a certain altitudes, $L \sim 1 - 10km$, the water vapour condenses into visible clouds, while the cooler air falls towards the sea. This ciruclation is organised into parallel rotating parallel columns of air, forming distinct cloud streets.

The common thread among the examples discussed above is the interaction between shear and bouyancy forces driven fluid motion - the central focus of this thesis. By restricting our analysis to these two mechanisms, we neglect other physical mechanisms such as phase change, chemical reactions and evaporation, which may be significant in the context of cooling microproccessors, chemical vapour deposition, and atmopsheric boundary layers respectively [Vallis et al., 2019]. To consider this

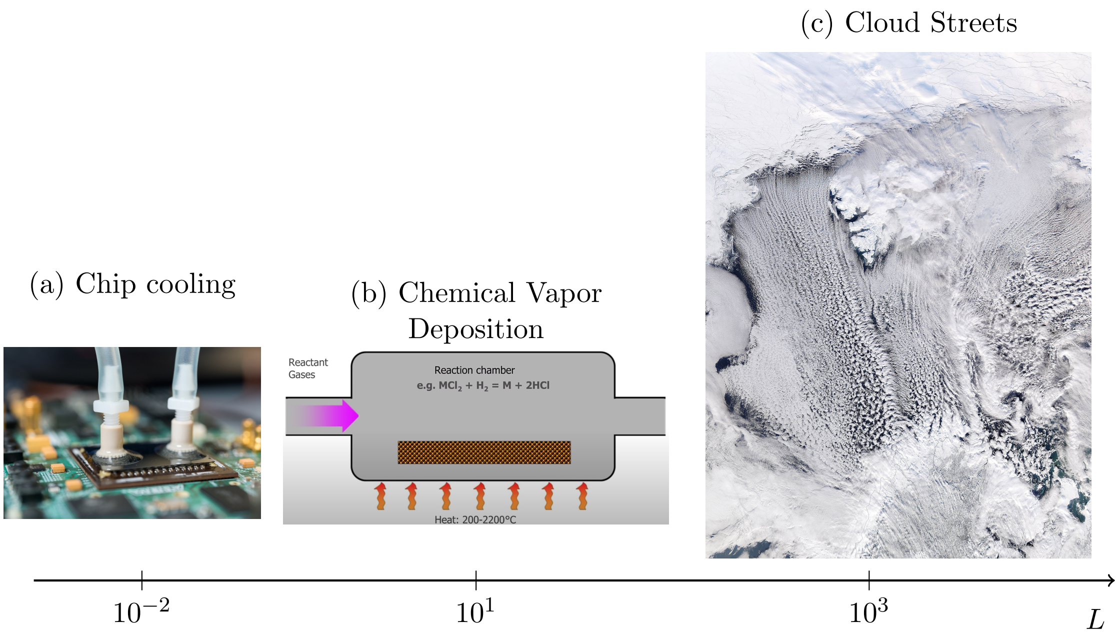

Figure 1.1: Fluid flow due to shear and bouuyancy forces across length scales, $L \in [1cm, 1km]$, such as (a) chip cooling, (b) chemical vapour deposition and (c) formation of cloud streets.

interaction, we consider an idealised setup without geometric complexity, known to as the Rayleigh-Bénard-Poiseuille (RBP) flow. This system describes the fluid motion confined between two infinitely extended parallel plates, heated from below and cooled from the top, with an additional pressure gradient driving the flow. The RBP configuration combines two paradigmatic flow configurations; the classical Rayleigh-Bénard convection (RBC), driven purely by buoyancy, and plane Poiseuille flow (PPF), driven purely by shear. While the onset of convection in RBC, and the transition to subscritical shear-driven turbulence in PPF have been both extensively studied, the transitional regime in which both forces interact remains less understood. Gaining insights into this regime can have implications for various applications across a range of scales mentioned previously.

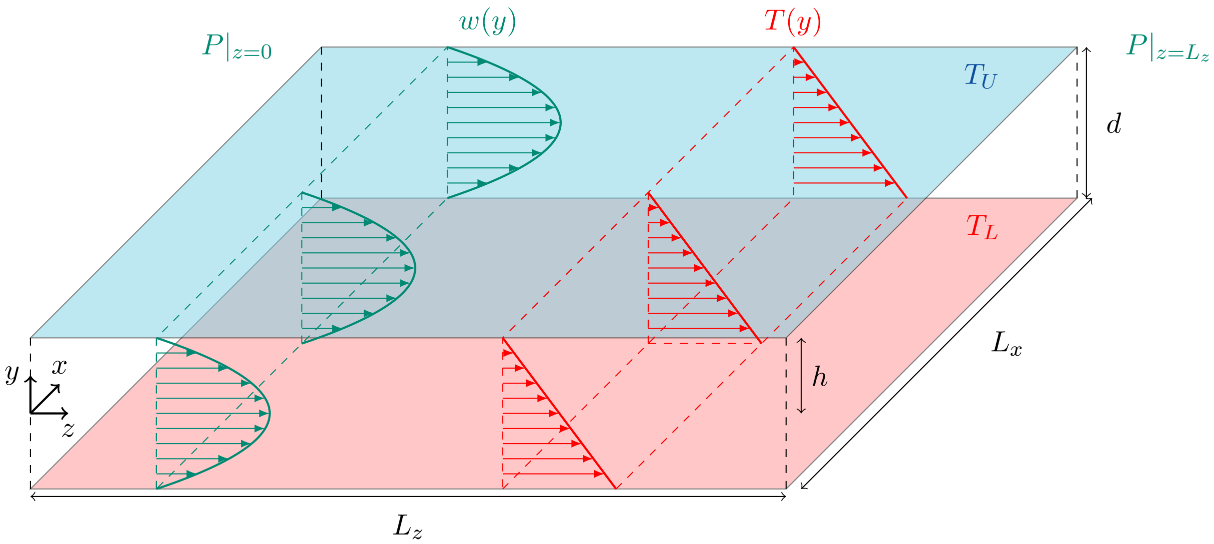

Figure 1.2: The Rayleigh-Bénard Poiseuille (RBP) flow configuration.

The RBP configuration is illustrated in figure 1.1, where $z^*, y^*, x^*, L_z, L_x, d, h$ refer to the streamwise, spanwise, wall-normal coordinates, length, span, depth and half-height of the domain respectively. We note that the asterisks*, refer to variables in dimensional form. The flow is driven by a pressure gradient along the streamwise z^* direction, $\Delta P^* = P^*|_{z^*=0} - P^*|_{z^*=L_z} < 0$, leading to the formation of a laminar Poiseuille flow, $w^*(y^*)$, for a sufficiently small ΔP. In this study, we will only consider fully-developed flow, where the boundary layer from the top and the bottom wall meets at the midplane, $y^* = 0$, and entrance effects are neglected. The RBP configuration is also unstably stratified, such that the temperature difference between the lower, T_L, and upper wall, T_U, is always positive, $\Delta T = T_L - T_U > 0$, leading to a stable linear conduction profile along the wall-normal direction, $T(y^*)$, if ΔT is kept sufficiently small.

In the absence of a pressure gradient, the RBP configuration reduces to the classical Rayleigh-Bénard convection problem, bringing about buoyany-driven convection for a sufficiently large unstable stratification. In the limiting case without unstable stratification, $\Delta T = 0$, the system reduces to the wall-bounded plane Poiseuille flow (PPF), where the transition towards subscritical shear-driven turbulence may be expected for a sufficiently large pressure gradient.

For instance, do buoyancy forces promote the transition to shear-driven turbulence and how does shear influence the convection? To describe the motion of the fluid in RBP configurations, we cosider non-dimensionalised Navier-Stokes equations with Boussinessq approximations,

$$\frac{\partial \mathbf{u}}{\partial t} + (\mathbf{u} \cdot \nabla)\mathbf{u} = -\nabla p + \frac{1}{Re}\nabla^2 \mathbf{u} + \frac{Ra}{Re^2 Pr}\theta, \tag{1.1a}$$

$$\frac{\partial \theta}{\partial t} + (\mathbf{u} \cdot \nabla)\theta = \frac{1}{RePr}\nabla^2 \theta, \tag{1.1b}$$

$$\nabla \cdot \mathbf{u} = 0. \tag{1.1c}$$

where $\mathbf{u}(\mathbf{x}), \theta(\mathbf{x}), p(\mathbf{x})$ refers to the nondimensionalised velocity, temperature and presure respectively. The key control parameters for RBP flows are the Rayleigh number, Ra, Reynolds number, Re, Prandlt number Pr, which are defined as follows,

$$Ra = \eta g d^3 \Delta T/\nu\kappa, \quad Re = W_c h/\nu, \quad Pr = \kappa/\nu, \quad \Gamma = L/2d, \tag{1.2}$$

where $\eta, g, \Delta T, \nu, \kappa, W_c, h, d, L$ are the thermal expansion coefficient, acceleration due to gravity, temperature difference between the bottom and top wall, kinematic viscosity, thermal diffusivity, laminar centreline velocity, domain's half-depth, full-depth, length or span respectively.

We describe important historical of hydrodynamic stability of planar shear flows and their theorectical frameworks in §1.2. Theorectical frameworks used in the study of stability of flow such as linear stability, nonlinear dynamical systems and spatiotemporal character of transitional shear flows will be outlined. This followed the historical developments of Rayleigh-Bénard convection (RBC), where concepts of the stability of fluid flows will be ultilised in §1.3. After which, we describe the historical developments of RBP flows §1.4, and the outline of the thesis will be give in §1.4.1.

1.2 Transitional wall-bounded shear flows

Wall-bounded shear flows concerns the motion of the fluid flowing in parallel to walls, typically bounded by one or more walls. The fluid closest to the wall comes to a rest, satisfying the no-slip boundary condition in the presence of a wall. As a consequence, a velocity gradient in the direction perpendicular from the wall develops, where the fluid layer becomes *sheared* due to the pressence of the wall - referred to wall-bounded sheared flows. Example of wall-bounded shear flows include the pressure-driven plane Poiseuille flow (or channel flow), Hagen-Poiseuille (or pipe) flows, plane Couette flow and flat plate boundary layers. These geometrically simple examples enables a convenient framework amenable to the mathematical analysis of fluid motion subjected to shear. Depending on the degree of shear, the fluid motion can be either laminar, where the fluid layers move in smooth parallel 'laminates', or turbulent, characterised by chaotic eddying motions. We also note that there is a transitional regime where both states can coexist discuss later. A central question is predicting the transition from the laminar regime to the turbulence.

The earliest investigation into this transition dates back to the pipe flow experiments of Reynolds [1883]. In his experimental setup, the flow speed through the pipe could be controlled by regulating the inlet pressure, while injecting dye to visualise the flow, as illustrated in figure 1.3(a). At low speeds, the fluid remained laminar, resulting to a single streak of steady dye in figure 1.3(b). As the speed increased, the dye begin to exhibit irregular 'sinuous' motions interspersed with laminar regions shown in figure 1.3(c). This is now referred to as the transitional/intermittent regime, alternating between the laminar and turbulent states. Beyond a critical speed, the dye breaks down entirely into chaotic 'eddies', mixing with the surrounding fluid and discolouring the flow with dye downstream in figure 1.3(d). This regime is now identified as turbulence.

Reynolds conjectured that the threshold between the laminar, transitional and turbulent regimes could be characterised by the Reynolds number, $Re = UD/\nu$, where U is the centerline velocity in the pipe, D, the pipe diameter and ν, the kinematic viscosity. He observed that flow through the pipe remained 'stable' and laminar for $Re < 1900$, while it became 'unstable' and turbulent for $Re > 2000$ [Reynolds, 1895]. His remarks led to the concept of the stability of fluid flows.

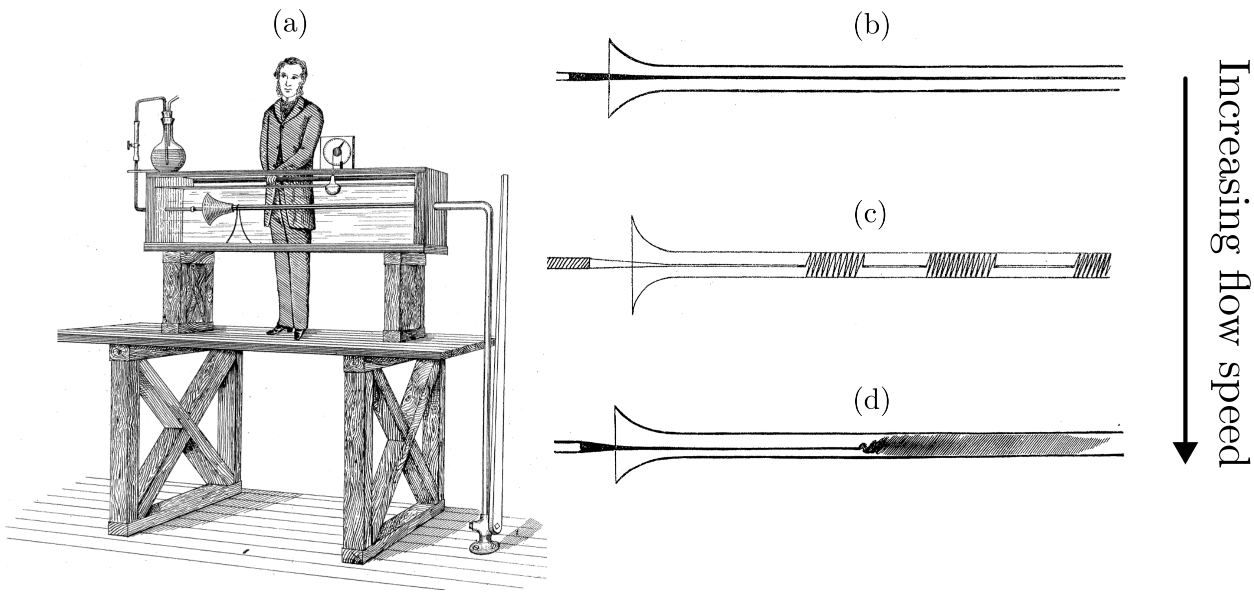

Figure 1.3: (a) Osbourne Reynolds pipe experiment with the dye injection apparatus, illustrating the (b) laminar flow, (c) intermittent regime and (d) turbulent flow as the flow speed is increased, taken from [Reynolds, 1883].

1.2.1 Linear Stability Analysis

Following Reynolds' experiment, interest towards the mathematical analysis of the stability of fluid flows grew in early 20^{st} century. The mathematical approach typically begins by decomposing the velocity field, $\mathbf{u}(\mathbf{x},t)$, into a laminar (base) state, $U(y)$ (assumed to depend only on the wall-normal direction here), and the velocity perturbations, $\mathbf{u}'(\mathbf{x},t)$, with pressure similarly decomposed as,

$$\mathbf{u}(\mathbf{x}) = U(y) + \mathbf{u}'(\mathbf{x},t), \quad \text{and} \quad p(\mathbf{x},t) = P(x) + p'(\mathbf{x},t). \tag{1.3}$$

Next, we the substitute the formulations for the decomposed velocity and pressure into the Navier-Stokes equations of equation (1.1) and drop the nonlinear pertubrations terms $(\mathbf{u}' \cdot \nabla)\mathbf{u}'$,

$$\frac{\partial \mathbf{u}'}{\partial t} + (U \cdot \nabla)\mathbf{u}' + (\mathbf{u}' \cdot \nabla)U = -\nabla p' + \frac{1}{Re}\nabla^2 \mathbf{u}', \tag{1.4a}$$

$$\nabla \cdot \mathbf{u}' = 0, \tag{1.4b}$$

resulting to the linearised Navier-Stokes equations. This commonly followed by introducing a wavelike ansatz (mode) defined by streamwise and spanwise wavenumbers, α, β and complex frequency, ω. In general two ways to analysis the linearised Navier-Stokes equations by considering the behaviour of each mode independently in §1.2.1 and their coupled dynamics in §1.2.1

Modal analysis

It is covenient to eliminate the pressure terms by to transform equation (1.4) using the wall-normal perturbation velocity, v', and wall-normal vorticity, $\eta' = \partial u'/\partial z - \partial w'/\partial x$, variables. Using (v, η), introduce an ansatz (mode) for them,

$$v'(\mathbf{x},t) = \tilde{v}(y)e^{i(\alpha x + \beta z - \omega t)}, \quad \text{and} \quad \eta'(\mathbf{x},t) = \tilde{\eta}(y)e^{i(\alpha x + \beta z - \omega t)}. \tag{1.5}$$

where α, β, ω denotes the streamwise and spanwise wavenumbers, and complex frequency (i.e. $\omega = \omega_r + i\omega_i$), respectively. Next, we substitute the ansatz into equation 1.4, leading to the classical Orr-Sommerfeld and Squire equations [Orr, 1907, Sommerfeld, 1909, Squire, 1933, Schmid and Henningson, 2001],

$$\left[-i\omega \begin{pmatrix} k^2 - \mathcal{D}^2 & 0 \\ 0 & 1 \end{pmatrix} + \begin{pmatrix} \mathcal{L}_{OS} & 0 \\ i\beta U' & \mathcal{L}_{SQ} \end{pmatrix}\right] \begin{pmatrix} \tilde{v} \\ \tilde{\eta} \end{pmatrix} = \mathbf{0}, \tag{1.6}$$

where $\mathcal{L}_{OS}$ and $\mathcal{L}_{SQ}$ refers to the Orr-Sommerfeld and Squire operators given as,

$$\mathcal{L}_{OS} = i\alpha U(k^2 - \mathcal{D}^2) + i\alpha U'' + \frac{1}{Re}(k^2 - \mathcal{D}^2)^2, \tag{1.7a}$$

$$\mathcal{L}_{SQ} = i\alpha U + \frac{1}{Re}(k^2 - \mathcal{D}^2). \tag{1.7b}$$

$k^2, \mathcal{D}, U', U''$ denotes the sum of squared wavenumbers, $k^2 = \alpha^2 + \beta^2$, differential operator in y, first- and second- derivative of the laminar velocity, respectively. Equation (1.6) is simply an eigenvalue problem which could be represented as,

$$\mathbf{L}\tilde{\mathbf{q}} = i\omega \mathbf{M}\tilde{\mathbf{q}} \tag{1.8}$$

where,

$$\mathbf{L} = \begin{pmatrix} \mathbf{L}_{OS} & 0 \\ i\beta U' & \mathcal{L}_{SQ} \end{pmatrix}, \quad \mathbf{M} \begin{pmatrix} k^2 - \mathcal{D}^2 & 0 \\ 0 & 1 \end{pmatrix}, \quad \tilde{\mathbf{q}} = \begin{pmatrix} \tilde{v} \\ \tilde{\eta} \end{pmatrix}. \tag{1.9}$$

and $i\omega$ refers to the eigenvalue. The aim of linear stability analysis is to determine the critical Reynolds number, Re_c, which is defined as the lowest value of Re over α and β, such that $Im[\omega] = 0$. For $Re > Re_c$, perturbations could grow exponentially, departing from the laminar state. In other words, we consider the behaviour of each $\alpha - \beta$ mode independently, herein referred to as *modal* analysis. Squire's theorem implies that for any unstable three-dimensional perturbations, $\beta \neq 0$, there exist an unstable two-dimensional perturbation, $\beta = 0$ with a lower Re_c [Squire, 1933]. Therefore, the unstable perturbations of wall-bounded shear flows at Re_c must be two-dimensional. The theoretical calculations was first perform by Tollmien [1928] and Schlichting [1933] for a flat-plate boundary layer flow, yielding a critical Reynolds number based on streamwise distance x of $Re_{x,c} = Ux_c/\nu = 520$ [Schlichting and Gersten, 2017]. In their honour, the unstable two-dimensional perturbations of the Orr-Sommerfeld operator is referred to as Tollmien-Schlicting (T.S) waves. For plane Poiseuille flow [Orszag, 1971] with a critical wavenumber of $\alpha_c = 1.02$. However, turbulence in plane Poiseuille flows have been observed at much lower Reynolds number, $Re \sim 1000 - 2000$, contradicting the results from linear stability analysis. Likewise, the onset of turbulence appear near $Re_{x,c} \approx 5 \times 10^5$ for flat plat boundary layer. A similar result holds for the plane Couette flow [Meseguer and Trefethen, 2003]. Despite its limitation, linear analysis analysis succeeds in predicting the critical Rayleigh number in Rayleigh-Bénard convection.

Non-modal stability

One of a major limitation of linear stability analysis considered above is that it treats each eigenmode independently, referred to as *modal* analysis. However, the interaction between decaying eigenmodes may lead to a short-term amplification of perturbations, before eventually decaying. This phenomenon is referred to as *transient growth*, and the method of analysis is referred to as *non-modal* analysis, related to the normality of the linear Orr-Sommerfeld operator [Schmid, 2007]. To demonstrate an

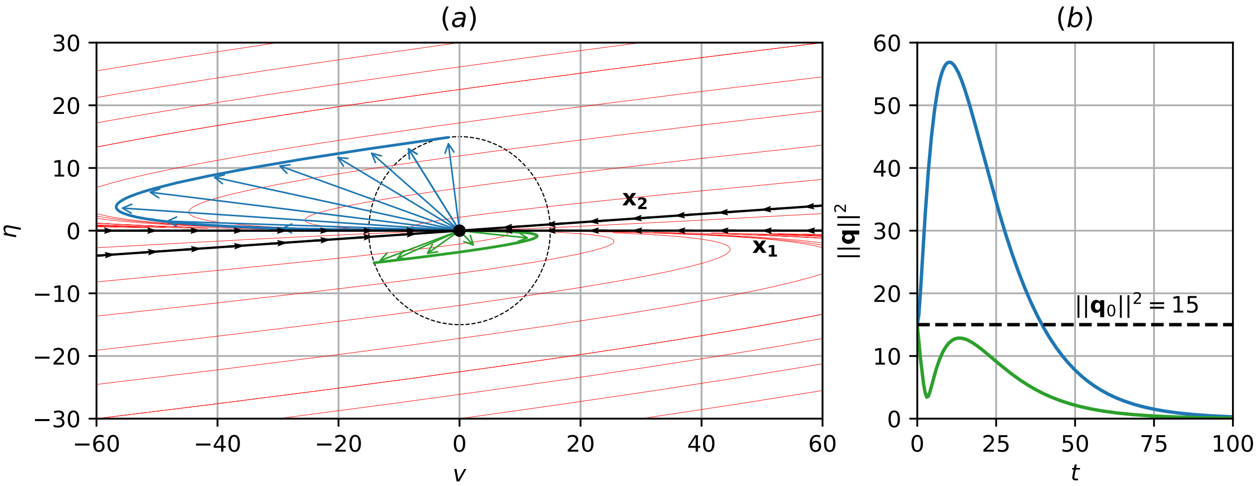

Figure 1.4: (a) The phase portrait of the toy model with $Re = 15$, (b) Transient growth.

example of transient growth, we consider a two-dimensional toy model governing the time-evolution of $\mathbf{q}$,

$$\frac{\mathrm{d}}{\mathrm{d}t}\begin{pmatrix} v \\ \eta \end{pmatrix} = \begin{pmatrix} -\frac{1}{Re} & -1 \\ 0 & -\frac{2}{Re} \end{pmatrix}\begin{pmatrix} v \\ \eta \end{pmatrix}, \tag{1.10}$$

where Re refers to the Reynolds number. The toy model is has negative eigenvalues, $(\lambda_1, \lambda_2) = (-1/Re, -2/Re)$, and unit eigenvectors $\mathbf{x_1} = (1, 0)$, $\mathbf{x_2} = \frac{1}{\sqrt{Re^2+1}}(Re, 1)$. Judging from the negative eigenvalues, we conclude that $\mathbf{q}(t)$ will decay exponentially. However, as $Re \to \infty$, they becoming increasingly non-orthogonal approaching each other such that the angle between $\mathbf{x}_1$ and $\mathbf{x}_2$ tend towards 0. At $Re = 15$, the eigenvector pairs, $\mathbf{x_1}$ and $\mathbf{x_2}$, are highly non-orthogonal, becoming almost linear dependent shown in figure 1.4(a). For a randomly selected initial condition with an energy-norm of $||\mathbf{q}_0||_2 = 15$, where $||\cdot||_2$ refers to the L2-norm, the trajectory in green decays exponentially for $t \in [0, 100]$ in figure 1.4(b). In constrast, for a specifically chosen initial condition in shown as the blue trajectory, $||\mathbf{q}||_2$ is amplified nearly four times before decaying exponentially. The toy model demonstrates the significance of transient growth for a specifically chosen initial condition.

The goal of non-modal stability analysis is to searching over all initial conditions, $\tilde{\mathbf{q}}_0$, leading to the maximum amplification factor at time t, resulting in an optimisation problem,

$$G(t) = \max_{\tilde{\mathbf{q}}_0 \neq 0} \frac{\langle \tilde{\mathbf{q}}(t), \tilde{\mathbf{q}}(t) \rangle}{\langle \tilde{\mathbf{q}}_0, \tilde{\mathbf{q}}_0 \rangle}, \quad \text{s.t} \quad \langle \tilde{\mathbf{q}}_0, \tilde{\mathbf{q}}_0 \rangle = 1, \tag{1.11}$$

where, $\langle \cdot, \cdot \rangle$ refers to the inner-product defined as,

$$\langle \mathbf{x}, \mathbf{y} \rangle = \int_\Omega \mathbf{x}^H \mathbf{y} \, \mathrm{d}\Omega, \tag{1.12}$$

and $\mathbf{x}^H$ refers to the complex conjugate transpose of $\mathbf{x}$. By considering the linearised operator of (1.6), we can define a linear time invariant operator given as,

$$\tilde{\mathbf{q}}(t) = \mathcal{A}(t)\tilde{\mathbf{q}}_0, \tag{1.13}$$

which takes the solution from initial conditions, $\tilde{\mathbf{q}}_0$, to $\tilde{\mathbf{q}}(t)$ at time t. Subtituting the expression above into equation (1.11),

$$G(t) = \max_{\tilde{\mathbf{q}}_0 \neq 0} \frac{\langle \mathcal{A}(t)\tilde{\mathbf{q}}_0, \mathcal{A}(t)\tilde{\mathbf{q}}_0 \rangle}{\langle \tilde{\mathbf{q}}_0, \tilde{\mathbf{q}}_0 \rangle} = \langle \tilde{\mathbf{q}}_0, \mathcal{A}^\dagger(t)\mathcal{A}(t)\tilde{\mathbf{q}}_0 \rangle = \lambda_{max}(\mathcal{A}^\dagger \mathcal{A}) \tag{1.14}$$

where $\mathcal{A}^\dagger(t)$ refers to the adjoint of $\mathcal{A}(t)$. The maximum amplification factor $\max G(t)$ is the largest eigenvalue, λ_{max}, of $\mathcal{A}^\dagger\mathcal{A}$, and the eigenvalue problem is given as,

$$\mathcal{A}^\dagger(t)\mathcal{A}(t)\tilde{\mathbf{q}}_0 = \lambda\tilde{\mathbf{q}}_0, \tag{1.15}$$

where $\tilde{\mathbf{q}}_0$ refers to the eigenvector denoting the optimal initial condition. For a detailed derivation of the optimal initial conditions or forcing, the reader is referred to [Butler and Farrell, 1992, Schmid, 2007]. An alternative method of computing transient growth is computing the pseudospectral of linear operators discussed in [Trefethen, 1997], outside the scope of this thesis.

Both two-dimensional, $\beta = 0$, and three-dimensional, $\beta \neq 0$, non-modal stability analysis have been studied.

In the two-dimensional form, the optimal initial conditions are in the form of near wall vorticies tilted upstream, transiently energised referred to as the Orr-mechanism [Orr, 1907, Farrell, 1988, Reddy et al., 1993]. In the three-dimension form, streamwise vortices, acting as optimal initial conditions lead to the optimal response in the form of streamwise streaks [Reddy and Henningson, 1993]. Contrary to linear stability analysis which confers two-dimensional perturbations as linearly unstable, the key result in this analysis is that three-dimensional initial conditions, $\alpha = 0$, confer the optimal initial conditions leading to large transient growth at subcritical Reynolds numbers. Figure.. shows this.

The width of the streaks happen to be robustly occur around 100 wall units, the characteristics spacing identified in many experiments [Kline, Panton, Bandybopobi]

The optimal initial conditions involve streamwise vortices which amplify streaks, related to the lift-up effect [Ellingsen and Palm, 1975, Brandt, 2014]. These modal and nonmodal mechanisms above highlight developments based on linear methods.

1.2.2 Nonlinear dynamical systems

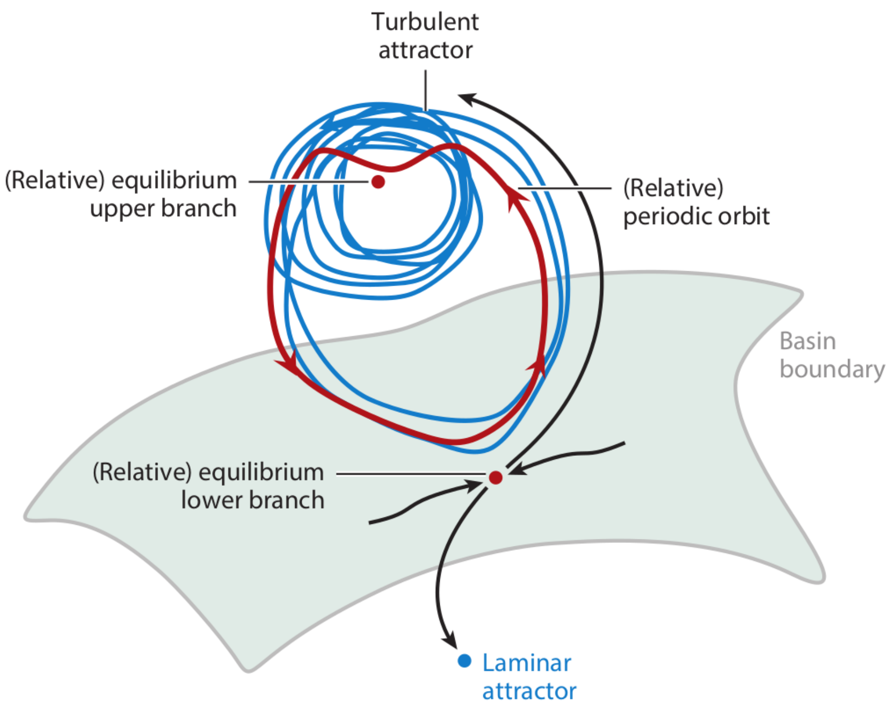

Figure 1.5: The state space organising of the upper and lower branch. Turbulence is interpreted as solution trajectories wander around the upper branch, orbiting around a network unstable invariant states. The lower branch acts as a boundary between the turbulent attractor and laminar attractor, an attracttor on the edge referred to as the edge state. Taken from [Graham and Floryan, 2021].

It is well established that coherent motions defined by flow patterns that persist in space and time play an important role in the transport of momentum and heat. In parallel shear flows, these coherent structures typically appear as near-walls streaks and quasi-streamwise rollers. A persistent, quasi-periodic cycle between the regeneration of streaks and rolls, referred to as the *self-sustaining process*, appears to be a fundamental mechanism in sustaining wall-bounded turbulence *self-sustaining process* [Hamilton et al., 1995]. This mechanism is described by the generation of streaks due to quasi-streamwise rollers by redistributing the mean. These streaks become linearly unstable and breakdown, and through a nonlinear process regenerates the quasi-streamwise rollers, closing the cycle.

In the previous section, we have examined the transition process based linear mechanisms. While such mechanisms are important, the transition to turbulence is ultimately governed fully nonlinear nature of the Navier-Stokes equations. As a result, an increasing attention has been directed towards the description of turbulence as a nonlinear dynamical systems. In this view, turbulence is interpreted as a solution trajectory evolving through a phase space composed of a network such non-trivial nonlinear solutions, commonly referred to as exact coherent states (ECS) or invariant solutions [Graham and Floryan, 2021]. These invariant solutions commonly take the form of as equilibria, travelling waves, periodic and relative periodic orbits.

In the context of parallel shear flows, Nagata was the first to discover a pair of unstable equilibirum solutions in plane Couette flow by smoothly following (homotopy) from a Taylor-Couette configuration [Nagata, 1990]. This pair consist of an unstable upper branch and lower branch emerging as a saddle-node bifurcation near $Re \approx 500$, and is disconnected from the stable laminar solution. The lower branch refers to its proximity towards the stable laminar state in phase space. A travelling-wave solution in plane Couette flow also later found by the same author [Nagata, 1997]. A family of equilibrium and travelling waves solutions was found for plane Couette and plane Poiseuille flows under various boundary conditions (i.e. stress-free, slip and no-slip) where identified by [Waleffe, 2001, 2003].

While these unstable solutions demonstrate good agreements with results from DNS such as the spanwise length scales, and mean and fluctuations, they do not capture the dynamical processes. Periodic orbits defined by time-dependent solutions that have been identified in plane Couette flow [Kawahara and Kida, 2001], describing a single regeneration cycle similar to the self-sustaining process. The chaotic trajectories of turbulence have been found to be embedded within invariant solutions and their connections between them known as heteroclinic orbits, offering a robust view of the building-blocks of of turbulence [Gibson et al., 2008, 2009, Viswanath, 2007, Halcrow et al., 2009, Graham and Floryan, 2021]

In the context of this transitional flows, the lower branch solution can be though of separating the turbulent attractor from the laminar state. Its an attractor that resides on the edge of turbulence, defined as an edge state. The graphical representation of this edge is shown in figure 1.5.

1.2.3 Spatiotemporal transitonal flows

This section describes the inherent spatiotemporal intermittent description of turbulence in transitional wall-bounded shear flows commonly reported in large extended domains where the span is about fifty times the half-height of a plane Poiseuille channel, $L/h \gtrsim 50$. In thie regime, turbulence is characterised by the coexistence of turbulent and laminar structures. Examples of such are found in canonical shear flow systems such as plane Couette flows [Prigent et al., 2003, Barkley and Tuckerman, 2005, 2007, Tuckerman and Barkley, 2011, Duguet et al., 2010, Reetz et al., 2019], Taylor-Couette flows [Prigent and Dauchot, 2002, Prigent et al., 2003], pipe flows [Avila et al., 2010, 2011, Song et al., 2017, Avila et al., 2023] and plane Poiseuille flows [Tsukahara et al., 2014a,c, Tuckerman et al., 2014, Tsukahara et al., 2014b, Gomé et al., 2020, Paranjape, 2019, Paranjape et al., 2020, 2023].

We will focus on the plane Poiseuille flow configuration, where the spatiotemporal intermittent patterns are referred to as oblique turbulent-laminar bands illustrated in figure 1.6 at $Re = 1400$ for $L/h = 16\pi$. The the bright and dark regions highlights coexisting spatially localised turbulent and laminar regions. These turbulent-laminar bands occur over a range of Reynolds numbers, and its precise range is likely dependent on the domain's aspect ratio [Tsukahara et al., 2014b, Tuckerman et al., 2014, Paranjape et al., 2023]. Near the upper Re threshold of this regime, the domain is

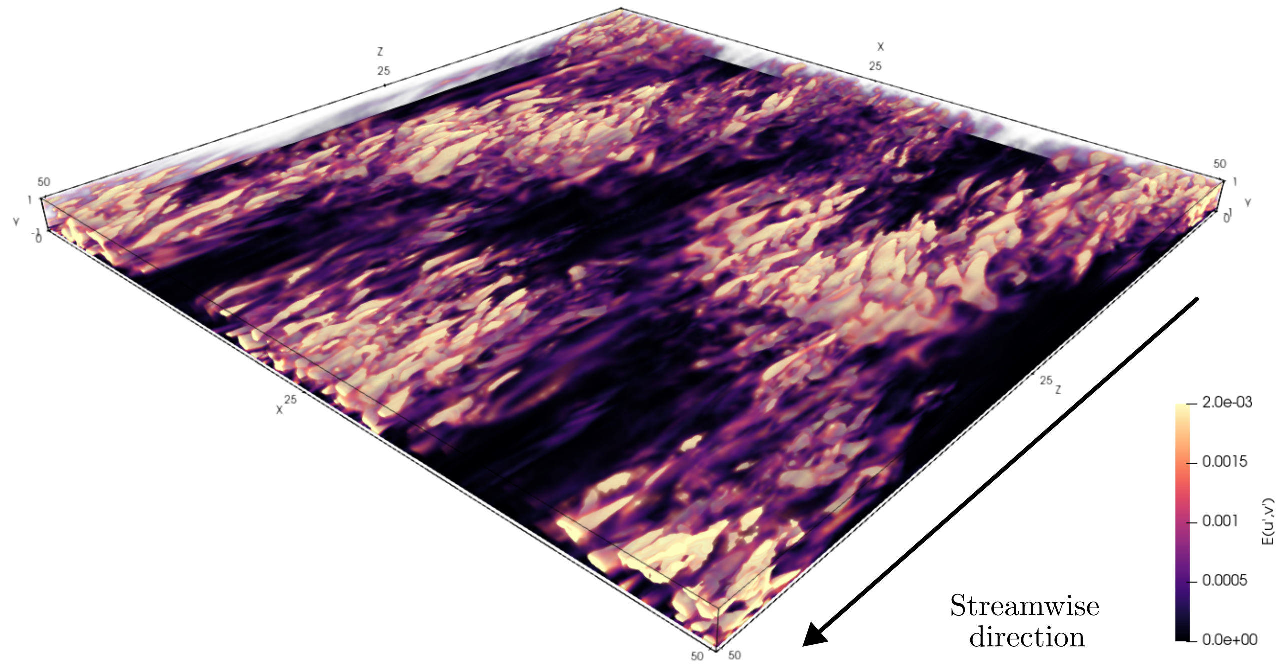

Figure 1.6: A snapshot of turbulent-laminar bands at $Re = 1400$ in a large domain $L/d = 8\pi$, depecting its spatiotemporal intermittent nature. Isovolume renderings is based on the spanwise, u', and wall-normal, v', perturbation kinetic energy, $E(u', v') = 1/2(u'^2 + v'^2)$, where the perturbation velocities are defined about the laminar state $\mathbf{u}'(\mathbf{x}, t) = \mathbf{u}(\mathbf{x}, t) - U_{lam}(y)$.

fully engulfed by developed turbulent regions, referred to uniform, featureless turbulence appearing at $Re = 1800$ in figure 1.6(a). As Re decreases towards $Re = 1050$, turbulent-laminar bands persist in figures 1.7(b-f). In this region, turbulent-laminar bands angles have been observed to be inclined between $20° \sim 30°$, with streamwise wavelengths of $\sim 60h$, and spanwise wavelengths of $\sim 20h - 30h$ [Tsukahara et al., 2014b]. To study the preference of angles, zzz performed linear stability analysis of bands and showed that preferred angle at .. degrees. Below certain Re threshold, the spatially turbulent regions spontaneously decay where the flow relaminarises asymptotically [Tuckerman et al., 2014]. This decay is shown in $Re = 1000$ near $t = 1600$ in figure 1.7(g).

Inspired from previous studies of turbulent-laminar bands in plane Couette flows [Barkley and Tuckerman, 2005, Reetz et al., 2019], narrow domains, titled orthogonally to the band angles where considered to investigate their dynamics [Tuckerman et al., 2014, Paranjape et al., 2020, 2023]. In narrow-tilted domains inclined at 24°, the turbulent-bands convect at about $\sim 1\%$ of the bulk velocity, propagating either upstream or downstream, above or below an critical $Re \sim 1000$, independent of domain sizes for $L_z \geq 100h$ [Tuckerman et al., 2014, Gomé et al., 2020]. The characteristic spanwise wavelengths of turbulent-laminar bands are depdendent on Re, appearing at $\lambda_z \sim 20h$ for $Re \geq 1400$ and $\lambda_z \sim 40h$ for $Re \leq 1100$. Indeed, between $1300 < Re < 1400$ the bands appear to alternative between two different band-widths [Tuckerman et al., 2014], merging and splitting continuously. This points towards a band splitting event in between $Re = 1100$ and $Re = 1400$, reminiscent of a puff

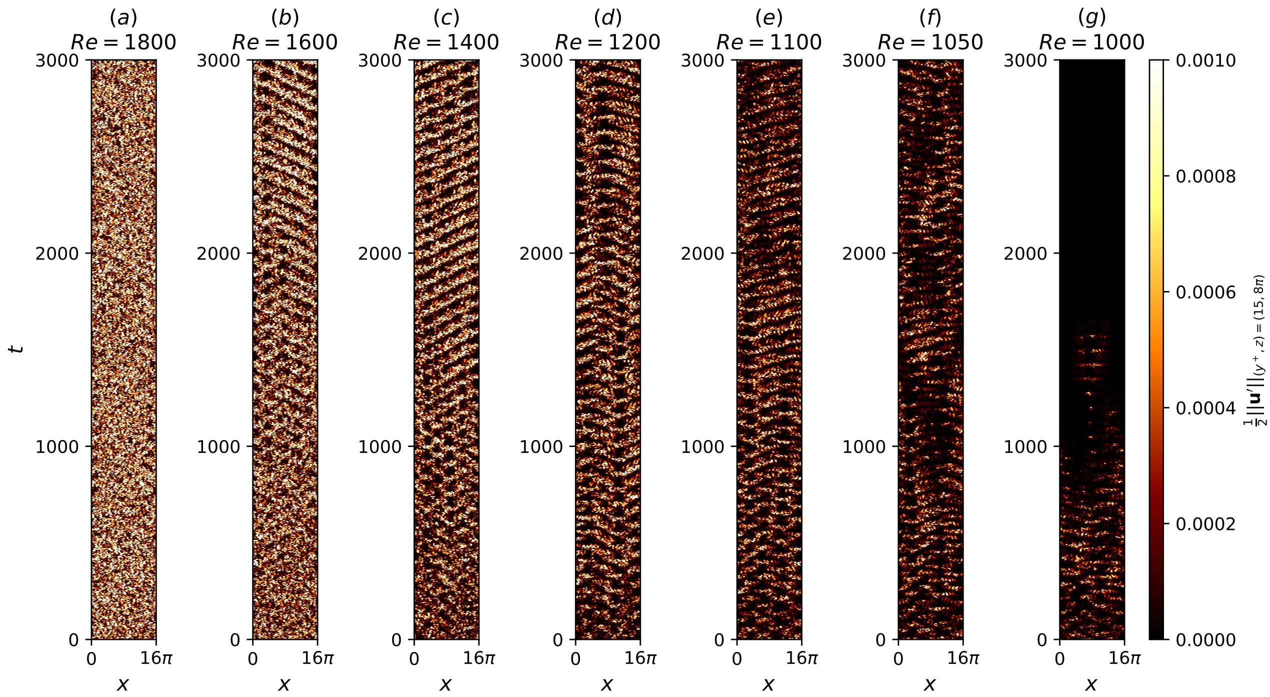

Figure 1.7: Turbulent-laminar bands for $t \in [0, 3000]$ in large domains $(L_x, L_z) = (16\pi, 16\pi)$ at (a) $Re = 1800$, (b) $Re = 1600$, (c) $Re = 1400$, (d) $Re = 1200$, (e) $Re = 1100$, (f) $Re = 1050$, (g) $Re = 1000$.

splitting in pipe flows [Avila et al., 2011].

On the other hand, turbulent bands appear to decay at $Re = 830$ [Gomé et al., 2020], and at $re = 1100$ but surviving for $re = 1000$ [Tuckerman et al., 2014], suggesting that turbulent bands decay spontaneously. [Gomé et al., 2020] computed the probabilities distributions of turbulent band decay, $P(\Delta t^d)$, where Δt^d refers to the time it takes for decay. On of the key insight is that the probability distributions of turbulent band decay mimicks a memoryless Poisson distribution,

$$P(\Delta t^d) = \exp(-\Delta t^d / \tau^d(Re)), \tag{1.16}$$

where $\tau^d(Re)$ refers to the mean lifetime for decay as a function of Re. Similarly, the probability distribution for band splitting also follows a Poisson distribution, $P(\Delta t^s) = \exp(-\Delta t^s/\tau^s(Re))$, where $\tau^s(Re)$ refers to the mean lifetime of a splitting event dependent on Re. The mean survival lifetime of a band decaying, τ^d, and splitting, τ^s, depends superexponentially on Re, i.e. $\tau^{d,s} = \exp(\exp(Re))$. This superexponential dependence is presented in figure 1.8, with a crossover point at $Re_{cross} \approx 965$. This crossover point refers to equal mean survival lifetime of a band de suggesting a critical Re for the onset of turbulent bands. While there has substantial progress made towards understanding the behaviour of periodic turbulent-laminar bands in narrow-tilted domains, recently studies of isolated turbulent bands (ITBs) indicate differed behaviour. Notably, ITBs persist at $Re \approx 700$ for $t = 10000$ (far beyond figure 1.8, characterised by streak generating head, and a diffusive upstream tail. [Xiong et al., 2015, Tao et al., 2018, Shimizu and Manneville, 2019, Xiao and Song, 2020].

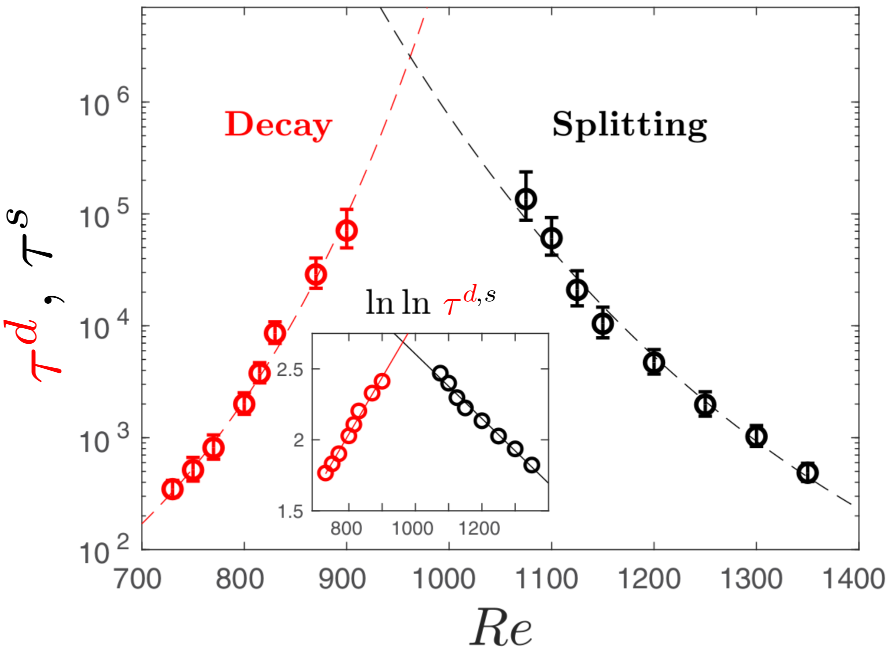

Figure 1.8: The mean decay times (red), τ^d, and mean splitting times (black), τ^s, as a function of Reynolds number, leading to a crossover point at $Re \approx 965$, adapted from [Gomé et al., 2020].

1.3 Rayleigh-Bénard convection

Rayleigh-Bénard convection (RBC) is a paradigmatic fluid configuration describing the motion of the fluid confined between two infinite-parallel plates heated from below and cooled from the top. As the bottom plate is heated, the bottom layer fluid becomes more buoyant and tends to rise, while the colder top fluid layer is becomes relatively less buoyant and tends to sink, leading to an overturning of layers. Viscous forces between neighbouring fluid parcels act to resist the motion. As buoyancy overcomes these viscous forces, the fluid layers overturn, resulting in the initiation of buoyancy-driven convection, the physical mechanism underpinning RBC.

One of the earliest experimental studies dedicated to buoyancy-driven convection was conducted by Henri Bénard [Bénard, 1901], who observed the formation of hexagonal convection cells above a certain temperature threshold ΔT. These hexagonal patterns are referred to as Bénard cells are illustrated in figure 1.9(a) (adapted from [Koschmieder and Pallas, 1974]). Subsequently, Rayleigh [1916] carried out one of first linear stability analyses of buoyancy-driven convection, predicting the onset of convection at a critical Rayleigh number of $Ra_c = 657.5$. However, Rayleigh's analysis assumed an idealised free-free boundary conditions, which differed from the rigid-free setup of Bénard's experiment. The linear stability analysis for rigid-free configuration was later performed by Jeffreys [1928] yielding a higher critical Rayleigh number of $Ra_c = 1058$. In the rigid-rigid configuration, the critical Rayleigh number increases further to $Ra_c = 1708$ [Pellew and Southwell, 1940]. The Rayleigh number in Bénard's original experiment was found to be 300 to 1500 smaller than Ra_c for the free-free and rigid-free cases [Wesfreid, 2017]. This contradiction, not recognised by Bénard at the time, lies in the significant role of surface tension in thin fluid layers exposed to air, now known as Bénard-Maragoni (BM) convection [Block, 1956, Cloot and Lebon, 1984, Manneville, 2006, Wesfreid, 2017]. In BM convection, fluid motion is primarily driven by surface tension gradients due to variations of temperature, forming hexagonal cells, as in figure 1.9(a). The preference for hexagonal cells in BM convection was later confirmed based on weakly nonlinear stability analysis [Cloot and Lebon, 1984].

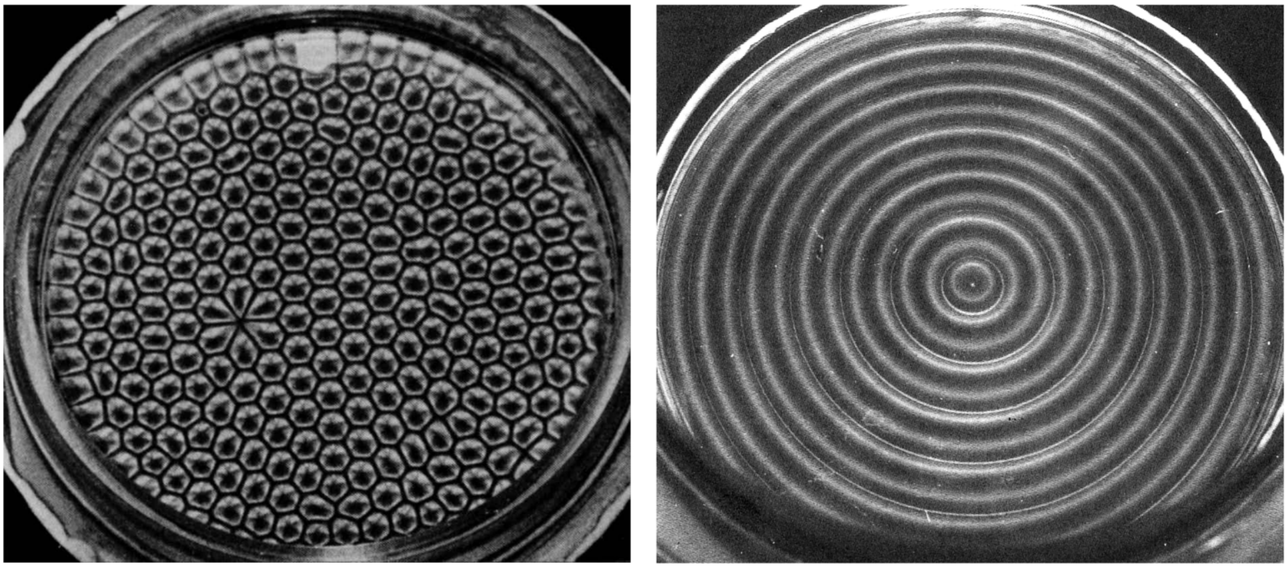

Figure 1.9: (a) Surface tension driven convection leading to the onset of hexagonal Bénard cells in a thin layer of silicone oil, heated from below and cooled by ambient air. A diamond defect appears, likely caused by plate imperfections. (b) Buoyancy driven convection in rigid plates, resulting to concentric convection rolls at 2.9 times the critical Rayleigh number. Both experiments were performed by Koschmieder and Pallas [1974], and the convection patterns were illuminated by aluminum powder, where the dark and bright regions refer to vertical and horizontal motions resepctively. These higher resolution images were taken from [Van Dyke and Van Dyke, 1982].

As the fluid layer becomes thicker, surface-tension effects diminish and buoyancy-driven convection becomes dominant. Similarly, placing a rigid lid on top of a thin fluid layer suppresses surface-tension effects, also resulting in buoyancy-driven convection. The preferred convection patterns based on weakly nonlinear stability analysis are the two-dimensional parallel rolls, now referred to as ideal straight rolls (ISRs) [Schlüter et al., 1965, Bodenschatz et al., 2000]. In circular ontainers, the ISRs conform to the geometry of the boundaries, forming of concentric convection rolls illustrated in figure 1.9(b). Interestingly, hexgaonal cells have been observed in buoyancy-driven flows of non-Boussinesq fluids [Hoard et al., 1970, Bodenschatz et al., 2000]. In this thesis, I will consider RBC with rigid-rigid boundary conditions with for which the critical Rayleigh number is $Ra_c = 1708$. Notably, the corresponding critical wavelength is $q_c = 3.12/d$ (or $\lambda_c \approx 2d$), suggesting that distance separating the plates, d, dictates the length of a single roll, $l_{roll} = \lambda_c/2 \approx d$.

As mentioned earlier, stationary ISRs near q_c emerge just above Ra_c, based on weakly nonlinear stabity analysis. [Eckhaus, 1965, Schlüter et al., 1965, Busse and Whitehead, 1971]. However, this prediction contradicted by the emergence of time-dependent oscillatory ISRs in experiments [Rossby, 1969, Willis and Deardorff, 1970] at $Ra = 9200$ (or roughly five times Ra_c), where weakly nonlinear stability becomes inapplicable. To address this, secondary stability analysis was employed to study the stability of ISRs further from Ra_c, based on Galerkin analysis [Busse, 1972] The results from the analysis is described by the Busse balloon, which illustrates the stability boundaries of ISRs as a function of Ra, Pr and roll wavenumber α in figure 1.10 [Busse, 1978]. The boundaries of the Busse balloon are described by various secondary instabilities, each arising from different physical mechanisms [Busse, 1978]. At lower wavenumbers, the zig-zag (ZZ) and cross-roll (CR) instabilities at high and intermediate Prandtl numbers. The ZZ instabilities cause zig-zag liked undulations of ISRs, while the CR instabilities lead to the formation of a roll orthogonal to the underlying ISRs.

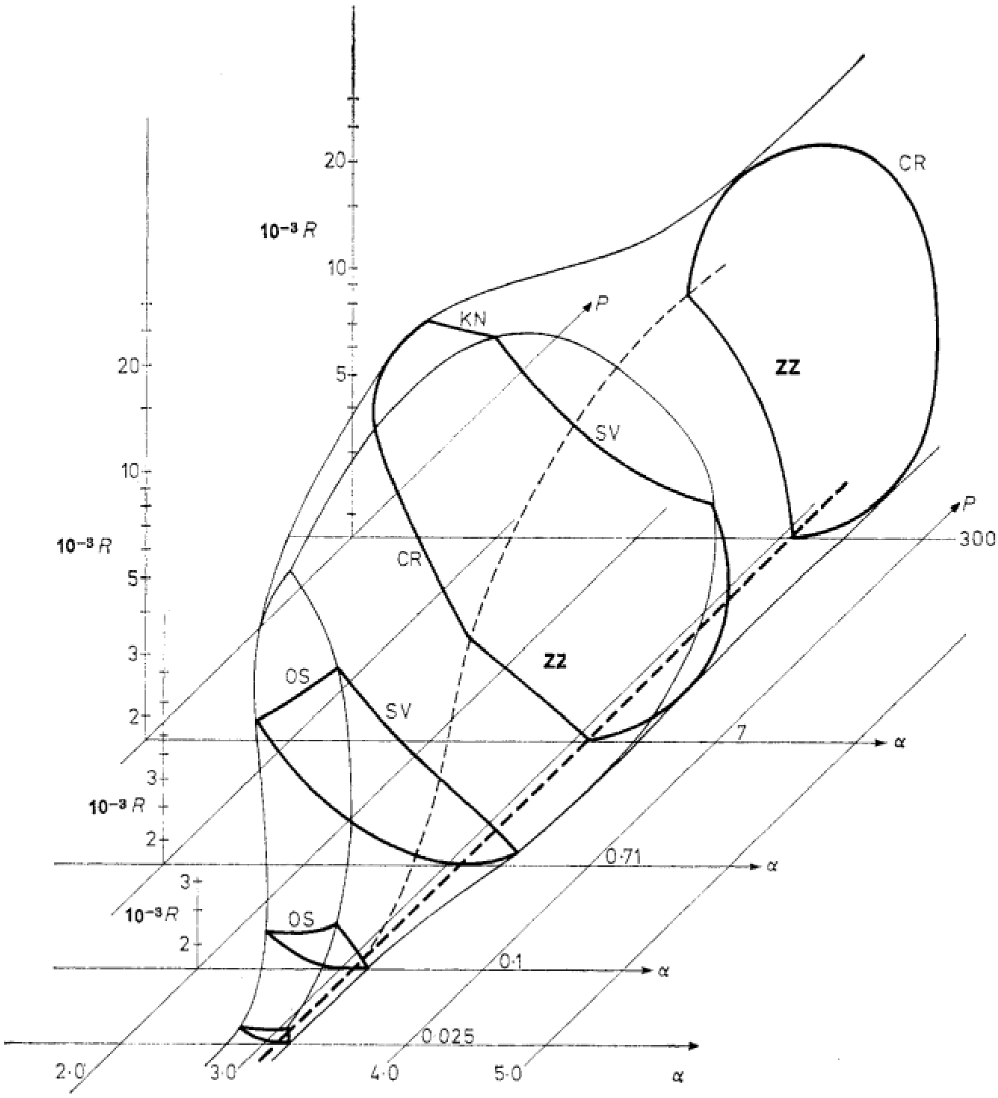

Figure 1.10: The Busse ballon describes the stability boundaries of ISRs in a $\varepsilon - q$ space. For larger wavenumbers, the instability mechanisms is described by the skewed-varicose (SV) instability. For smaller wavenumbers, the instability mechanism is described by the Eckhaus instability. For large ε, the instability is described by the onset of oscillatory instability. Busse balloon digitised from [Plapp, 1997] for $Pr \approx 1$

Both mechanisms increases the effective roll wavenumber, adhering within the stability boundaries. At higher wavenumbers, the skewed varicose (SV) instability becomes relevant at intermediate Prandlt numbers, characterised by roll pinching and merging that effectively reduces the roll wavenumber. For larger Rayleigh numbers and $Pr \lesssim 1$, the oscillatory instability (OS) arises, forming oscillatory ISRs [Willis and Deardorff, 1970]. In contrast, for higher Pr, the knot instability appears, modifying the cross-roll pattern into a spoke-like structure. In general, the Eckhaus instability (not shown) appears, acts to generate or destory rolls, adhering within the Busse balloon. In this thesis, we focus on at $Pr = 1$, where the skewed-varicose, Eckhaus and cross-roll instabilities typically arise.

While the Busse balloon describes the stability boundaries of ISRs over a range of wavenumbers, predicting the wavenumber of an ISR state remains an central challenge [Bodenschatz et al., 2000]. Indeed, experimental investigations of RBC in moderate domain sizes ($\Gamma \geq 7$, where Γ refers to the domain's aspect ratio) in rectangular (straight rolls) and cylinderical (concentric rolls) domains showed that the wavenumbers are confined within the Busse balloon. As ε is was continously modified, the ISRs with wavenumbers that are now outside of the Busse balloon, rolls dislocations and defects spontaneously nucleate, either increasing or decreasing the roll wavenumber, adhering to the the stability boundaries of the Busse balloon. The hysteretic nature of the system implies that the roll wavenumber of the ISRs strongly depends on the system's history [Bodenschatz et al., 2000].

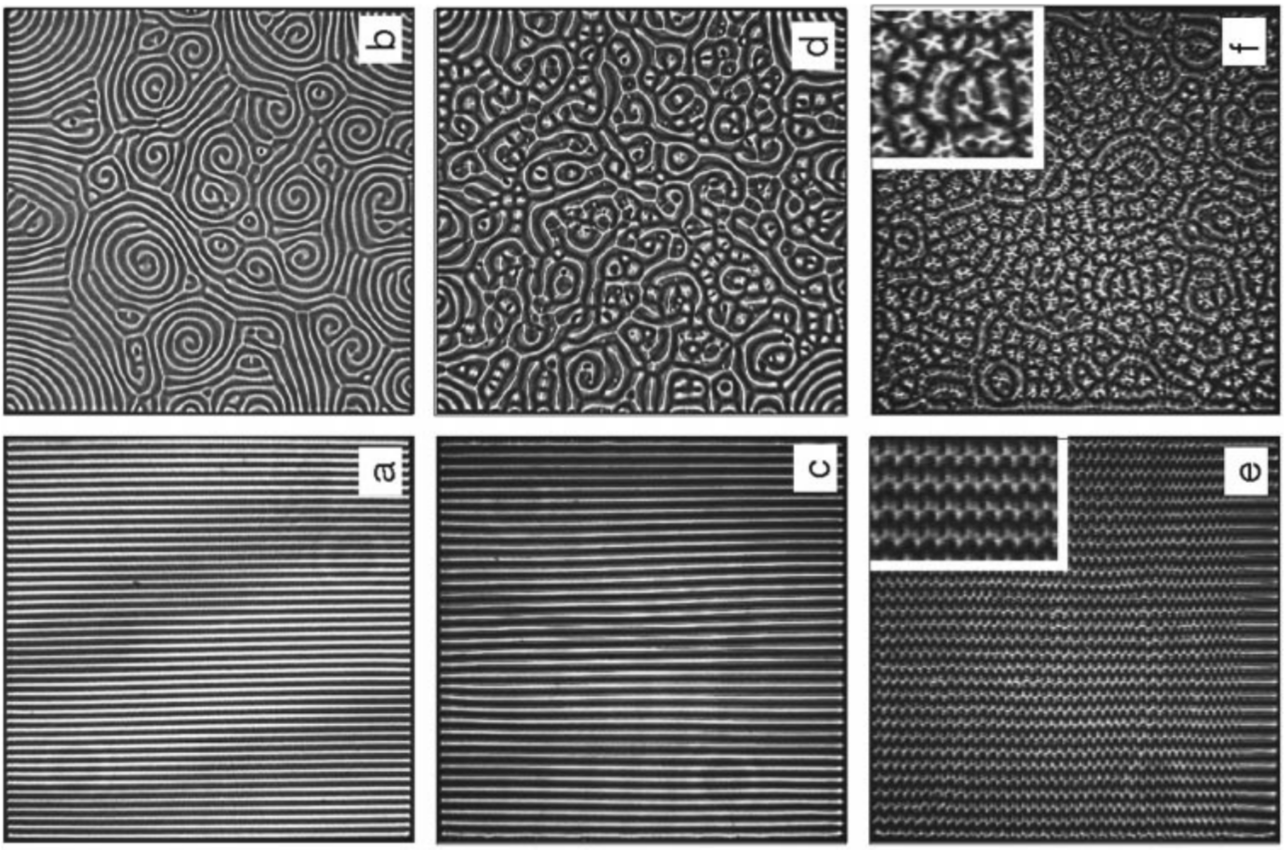

Figure 1.11: Spiral defect chaos (top row) coexisting with ISRs (bottom row) forming a bistable system.

It is worth noting that the solutions in the form of ISRs appear to be an exception rather than the rule [Croquette, 1989b]. The coexistence of multiple 'non-ISR' states, in the form of squares, travelling/stationary targets, giant rotating spirals, and oscillatory convection patterns have been found over several years [Le Gal et al., 1985, Croquette, 1989a, Plapp, 1997, Hof et al., 1999, Rüdiger and Feudel, 2000, Borońska and Tuckerman, 2010a,b]. Investigation of cylindrical RBC with small aspect-ratio ($\Gamma = 2$) found eight stationary states (at the same $Ra = 142000$), and two oscillatory states ($Ra > 14200$) [Hof et al., 1999]. These findings were later supported by numerical experiments and bifurcation analyses [Ma et al., 2006, Borońska and Tuckerman, 2010a,b]. In particular, bifurcation analyses performed by Ma et al. [2006], revealed twelve stable branches in the form of symmetric and asymmetric convection rolls near onset ($Ra \leq 2500$), with the potential emergence of hundreds of branches at higher Rayleigh numbers, $Ra \leq 30000$ [Borońska and Tuckerman, 2010b]. In larger domains ($\Gamma \geq 28$), giant rotating spirals were identified and thoroughly investigated [Plapp and Bodenschatz, 1996, Plapp et al., 1998]. Experimental and numerical studies of RBC with varying side-wall boundary conditions (i.e. thermally insulating, conducting an no-slip) [Tuckerman and Barkley, 1988, Siggers, 2003, Paul et al., 2003, Boullé et al., 2022], non-Boussinesq convection [Bodenschatz et al., 1992], and rotational effects [Hu et al., 1997] were investigated, where multiple states were also reported.

1.4 Rayleigh-Bénard Poiseuille (RBP) flows

Gage and Reid [1968] first investigated the primary instabilities of RBP flows, which can be determined by Re, Ra, Pr, and the planar x-z perturbations wavenumbers α, β respectively. For a given Ra and Pr, the neutral stability curves are limited by the development of Tollmien-Schlicting waves for $Re \geq Re_{TS} = 5772.22$ [Orszag, 1971], and convection rolls within $0 \leq Re < Re_{TS}$. Convection rolls can be categorised based on their orientation to the mean flow, namely, longitudinal ($\alpha = 0, \beta \neq 0$), transverse ($\alpha \neq 0, \beta = 0$) and oblique rolls ($\alpha \neq 0, \beta \neq 0$). The linearised system governing the onset of longitudinal rolls is analogous to the linearised RBC system, with a critical Rayleigh number, $Ra_{\parallel} = Ra_{RB} = 1708.8$ and critical wavenumber, $\alpha_{\parallel} = \alpha_{RB} = 3.13$ [Pellew and Southwell, 1940, Kelly, 1994], independent of Re and Pr. The critical Rayleigh number for oblique and transverse rolls matches that of RBC at $Re = 0$ due to horizontal isotropy, but increases as Re increases, depending on Pr, i.e., $Ra_{\perp} = f(Re, Pr)$ [Gage and Reid, 1968, Müller et al., 1992, Nicolas et al., 1997]. When spatially developing instabilities are considered, longitudinal rolls are always convectively unstable, and transverse rolls can become absolutely unstable [Müller et al., 1989, 1992, Carrière and Monkewitz, 1999]. Nonmodal stability analyses of subcritical RBP indicate that the optimal transient growth G_{max} increases gradually with Ra. The wavenumber of the optimal initial conditions, β_{max}, resembles that observed in shear flows [Reddy and Henningson, 1993], and gradually approaches the critical wavenumber of convection rolls, $\alpha_{\parallel}$, as Ra increases [John Soundar Jerome et al., 2012]. For $Re > 0$, the longitudinal rolls appear as the dominant primary instability [Gage and Reid, 1968]. Secondary stability analyses of longitudinal rolls reveal a wavy instability near $Re \sim 100$ [Clever and Busse, 1991], leading to wavy longitudinal rolls, which are convectively unstable [Pabiou et al., 2005, Nicolas et al., 2010]. The influence of finite lateral extensions in RBP flows on the stability of longitudinal and transverse rolls [Kato and Fujimura, 2000, Nicolas et al., 2000], as well as wavy rolls [Xin et al., 2006, Nicolas et al., 2010], has been reported. In finite streamwise extensions of RBP flows, the onset of convection rolls and the heat flux variations due to entrance effects have been investigated [Mahaney et al., 1988, Lee and Hwang, 1991, Nonino and Giudice, 1991]. More recently, shear-driven turbulence can enhance heat fluxes in turbulent RBP flows [Scagliarini et al., 2014, 2015, Pirozzoli et al., 2017]. RBP flows with sinusoidal heating and wavy walls have also been studied [Hossain et al., 2021]. For an in-depth discussion of RBP flows, see the reviews by Kelly [1994] and Nicolas [2002].

1.4.1 Thesis Outline

In this thesis, I am particularly focused on the transition behaviour of fluid flow driven by shear and bouyancy, addressing questions related to the onset of instabilities due to shear and buoyancy, and the (possible) competitive between shear and buoyancy driven instabilities. I would like to preface that while this thesis is dealing with onset of instabilities, it does not clearly indicate that the onset of such instabilities necessarily lead to turbulence, hence, for terminology sake, we shall be looking into transitional regimes where the fluid neither laminar nor turbulent. The main motivations are two-folds, both from an academic and applied point-of-view. Within academia, the onset and transition to turbulence in Rayleigh-Bénard Poiseuille flows remains poorly understand. Whilst there had been significant progress in our understand of transition to turbulence in independent setups, Rayleigh-Bénard convection and plane Poiseuille flows, their combined effects are not known. The thesis is structured into the follow, Chapter 1 is the introduction with literature review, chapter 2 methodology assosicated with the spectral/hp-element method, chapter 3 with results related to the the Rayleigh and Reynolds number sweep, chapter 4 with a specific focus on the bistability between spiral defect chaos and ideal straight rolls and finally chapter 5 with concluding remarks.

1. Academic motivation - flow structures, statistics, transition.
2. Application motivation - shear, heat transfer. Chip cooling, thin-film fabrication and atmospheric boundary layer.

We seek to investigate the influence of unstable stratification quantified by Rayleigh number Ra, on the behaviour tuburlent-laminar bands. The onset of convection occurs at a critical Rayleigh number of $Ra_c > 1708$, in the form of a pair of convection rolls. When aligned in the streamwise direction, the convection rolls are seemingly analogous to a pair of counter-rotating vortices, an optimal initial condition for transient growth. Our investigation naturally answers a few questions related to turbulent-laminar bands. For example, does the onset of turbulent-laminar bands, Re_{cr} decrease with increasing Ra? Do Ra-effects influence the structure of turbulent-laminar bands i.e band angle/width?

The answers to our research will have important implications Rayleigh-Bénard Poiseuille flows, ubiquitous in atmospheric, geophysical and engineering flows.

Bibliography

Clouds streets and comma clouds near svalbard. https://earthobservatory.nasa.gov/images/87749/clouds-streets-and-comma-clouds-near-svalbard.

Kerstin Avila, David Moxey, Alberto De Lozar, Marc Avila, Dwight Barkley, and Björn Hof. The Onset of Turbulence in Pipe Flow. *Science*, 333(6039):192–196, July 2011. ISSN 0036-8075, 1095-9203. doi: 10.1126/science.1203223. URL https://www.science.org/doi/10.1126/science.1203223.

Marc Avila, Ashley P. Willis, and Björn Hof. On the transient nature of localized pipe flow turbulence. *Journal of Fluid Mechanics*, 646:127–136, March 2010. ISSN 0022-1120, 1469-7645. doi: 10.1017/S0022112009993296. URL https://www.cambridge.org/core/product/identifier/S0022112009993296/type/journal_article.

Marc Avila, Dwight Barkley, and Björn Hof. Transition to Turbulence in Pipe Flow. *Annual Review of Fluid Mechanics*, 55(1):575–602, January 2023. ISSN 0066-4189, 1545-4479. doi: 10.1146/annurev-fluid-120720-025957. URL https://www.annualreviews.org/doi/10.1146/annurev-fluid-120720-025957.

Dwight Barkley and Laurette S. Tuckerman. Computational Study of Turbulent Laminar Patterns in Couette Flow. *Physical Review Letters*, 94(1):014502, January 2005. doi: 10.1103/PhysRevLett.94.014502. URL https://link.aps.org/doi/10.1103/PhysRevLett.94.014502. Publisher: American Physical Society.

Dwight Barkley and Laurette S Tuckerman. Mean flow of turbulent–laminar patterns in plane Couette flow. *Journal of Fluid Mechanics*, 576:109–137, 2007. ISSN 1469-7645. Publisher: Cambridge University Press.

Myron J. Block. Surface Tension as the Cause of Bénard Cells and Surface Deformation in a Liquid Film. *Nature*, 178(4534):650–651, September 1956. ISSN 0028-0836, 1476-4687. doi: 10.1038/178650a0. URL https://www.nature.com/articles/178650a0.

Eberhard Bodenschatz, David S. Cannell, John R. De Bruyn, Robert Ecke, Yu-Chou Hu, Kristina Lerman, and Guenter Ahlers. Experiments on three systems with non-variational aspects. *Physica D: Nonlinear Phenomena*, 61(1-4):77–93, December 1992. ISSN 01672789. doi: 10.1016/0167-2789(92)90150-L. URL https://linkinghub.elsevier.com/retrieve/pii/016727899290150L.

Eberhard Bodenschatz, Werner Pesch, and Guenter Ahlers. Recent Developments in Rayleigh-Bénard Convection. *Annual Review of Fluid Mechanics*, 32(1):709–778, January 2000. ISSN 0066-4189, 1545-4479. doi: 10.1146/annurev.fluid.32.1.709. URL https://www.annualreviews.org/doi/10.1146/annurev.fluid.32.1.709.

Katarzyna Borońska and Laurette S. Tuckerman. Extreme multiplicity in cylindrical Rayleigh-Bénard convection. I. Time dependence and oscillations. *Physical Review E*, 81(3):036320, March 2010a. ISSN 1539-3755, 1550-2376. doi: 10.1103/PhysRevE.81.036320. URL https://link.aps.org/doi/10.1103/PhysRevE.81.036320.

Katarzyna Borońska and Laurette S. Tuckerman. Extreme multiplicity in cylindrical Rayleigh-Bénard convection. II. Bifurcation diagram and symmetry classification. *Physical Review E*, 81(3):036321, March 2010b. ISSN 1539-3755, 1550-2376. doi: 10.1103/PhysRevE.81.036321. URL https://link.aps.org/doi/10.1103/PhysRevE.81.036321.

N. Boullé, V. Dallas, and P. E. Farrell. Bifurcation analysis of two-dimensional Rayleigh-Bénard convection using deflation. *Physical Review E*, 105(5):055106, May 2022. ISSN 2470-0045, 2470-0053. doi: 10.1103/PhysRevE.105.055106. URL https://link.aps.org/doi/10.1103/PhysRevE.105.055106.

Luca Brandt. The lift-up effect: The linear mechanism behind transition and turbulence in shear flows. *European Journal of Mechanics - B/Fluids*, 47:80–96, September 2014. ISSN 09977546. doi: 10.1016/j.euromechflu.2014.03.005. URL https://linkinghub.elsevier.com/retrieve/pii/S0997754614000405.

F. H. Busse. The oscillatory instability of convection rolls in a low Prandtl number fluid. *Journal of Fluid Mechanics*, 52(1):97–112, March 1972. ISSN 0022-1120, 1469-7645. doi: 10.1017/S0022112072002988. URL https://www.cambridge.org/core/product/identifier/S0022112072002988/type/journal_article.

F H Busse. Non-linear properties of thermal convection. *Reports on Progress in Physics*, 41(12): 1929–1967, December 1978. ISSN 0034-4885, 1361-6633. doi: 10.1088/0034-4885/41/12/003. URL https://iopscience.iop.org/article/10.1088/0034-4885/41/12/003.

F. H. Busse and J. A. Whitehead. Instabilities of convection rolls in a high Prandtl number fluid. *Journal of Fluid Mechanics*, 47(2):305–320, May 1971. ISSN 0022-1120, 1469-7645. doi: 10.1017/S0022112071001071. URL https://www.cambridge.org/core/product/identifier/S0022112071001071/type/journal_article.

Kathryn M. Butler and Brian F. Farrell. Three-dimensional optimal perturbations in viscous shear flow. *Physics of Fluids A: Fluid Dynamics*, 4(8):1637–1650, August 1992. ISSN 0899-8213. doi: 10.1063/1.858386. URL https://pubs.aip.org/pof/article/4/8/1637/402702/Three-dimensional-optimal-perturbations-in-viscous.

Henri Bénard. Les tourbillons cellulaires dans une nappe liquide. - Méthodes optiques d'observation et d'enregistrement. *Journal de Physique Théorique et Appliquée*, 10(1):254–266, 1901. ISSN 0368-3893. doi: 10.1051/jphystap:0190100100025400. URL http://www.edpsciences.org/10.1051/jphystap:0190100100025400.

Philippe Carrière and Peter A. Monkewitz. Convective versus absolute instability in mixed Rayleigh–Bénard–Poiseuille convection. *Journal of Fluid Mechanics*, 384:243–262, April 1999. ISSN 0022-1120, 1469-7645. doi: 10.1017/S0022112098004145. URL https://www.cambridge.org/core/product/identifier/S0022112098004145/type/journal_article.

R. M. Clever and F. H. Busse. Instabilities of longitudinal rolls in the presence of Poiseuille flow. *Journal of Fluid Mechanics*, 229(-1):517, August 1991. ISSN 0022-1120, 1469-7645. doi: 10.1017/S0022112091003142. URL http://www.journals.cambridge.org/abstract_S0022112091003142.

A. Cloot and G. Lebon. A nonlinear stability analysis of the Bénard–Marangoni problem. *Journal of Fluid Mechanics*, 145(-1):447, August 1984. ISSN 0022-1120, 1469-7645. doi: 10.1017/S0022112084003013. URL http://www.journals.cambridge.org/abstract_S0022112084003013.

Vincent Croquette. Convective pattern dynamics at low Prandtl number: Part I. *Contemporary Physics*, 30(2):113–133, March 1989a. ISSN 0010-7514, 1366-5812. doi: 10.1080/00107518908225511. URL http://www.tandfonline.com/doi/abs/10.1080/00107518908225511.

Vincent Croquette. Convective pattern dynamics at low Prandtl number: Part II. *Contemporary Physics*, 30(3):153–171, May 1989b. ISSN 0010-7514, 1366-5812. doi: 10.1080/00107518908222594. URL http://www.tandfonline.com/doi/abs/10.1080/00107518908222594.

Y. Duguet, P. Schlatter, and D. S. Henningson. Formation of turbulent patterns near the onset of transition in plane Couette flow. *Journal of Fluid Mechanics*, 650:119–129, May 2010. ISSN 0022-1120, 1469-7645. doi: 10.1017/S0022112010000297. URL https://www.cambridge.org/core/product/identifier/S0022112010000297/type/journal_article.

Wiktor Eckhaus. *Studies in Non-Linear Stability Theory*, volume 6 of *Springer Tracts in Natural Philosophy*. Springer Berlin Heidelberg, Berlin, Heidelberg, 1965. ISBN 978-3-642-88319-4 978-3-642-88317-0. doi: 10.1007/978-3-642-88317-0. URL http://link.springer.com/10.1007/978-3-642-88317-0.

T. Ellingsen and E. Palm. Stability of linear flow. *The Physics of Fluids*, 18(4):487–488, April 1975. ISSN 0031-9171. doi: 10.1063/1.861156. URL https://pubs.aip.org/pfl/article/18/4/487/459138/Stability-of-linear-flow.

Greg Evans and Ralph Greif. Unsteady three-dimensional mixed convection in a heated horizontal channel with applications to chemical vapor deposition. *International Journal of Heat and Mass Transfer*, 34(8):2039–2051, August 1991. ISSN 00179310. doi: 10.1016/0017-9310(91)90215-Z. URL https://linkinghub.elsevier.com/retrieve/pii/001793109190215Z.

Brian F. Farrell. Optimal excitation of perturbations in viscous shear flow. *The Physics of Fluids*, 31(8):2093–2102, August 1988. ISSN 0031-9171. doi: 10.1063/1.866609. URL https://pubs.aip.org/pfl/article/31/8/2093/966463/Optimal-excitation-of-perturbations-in-viscous.

K. S. Gage and W. H. Reid. The stability of thermally stratified plane Poiseuille flow. *Journal of Fluid Mechanics*, 33(1):21–32, July 1968. ISSN 0022-1120, 1469-7645. doi: 10.1017/S0022112068002326. URL https://www.cambridge.org/core/product/identifier/S0022112068002326/type/journal_article.

J. F. Gibson, J. Halcrow, and P. Cvitanović. Visualizing the geometry of state space in plane Couette flow. *Journal of Fluid Mechanics*, 611:107–130, September 2008. ISSN 0022-1120, 1469-7645. doi: 10.1017/S002211200800267X. URL https://www.cambridge.org/core/product/identifier/S002211200800267X/type/journal_article.

J. F. Gibson, J. Halcrow, and P. Cvitanović. Equilibrium and travelling-wave solutions of plane Couette flow. *Journal of Fluid Mechanics*, 638:243–266, November 2009. ISSN 0022-1120, 1469-7645. doi: 10.1017/S0022112009990863. URL https://www.cambridge.org/core/product/identifier/S0022112009990863/type/journal_article.

Sébastien Gomé, Laurette S. Tuckerman, and Dwight Barkley. Statistical transition to turbulence in plane channel flow. *Physical Review Fluids*, 5(8):083905, August 2020. ISSN 2469-990X. doi: 10.1103/PhysRevFluids.5.083905. URL https://link.aps.org/doi/10.1103/PhysRevFluids.5.083905.

Michael D. Graham and Daniel Floryan. Exact Coherent States and the Nonlinear Dynamics of Wall-Bounded Turbulent Flows. *Annual Review of Fluid Mechanics*, 53(1):227–253, January 2021. ISSN 0066-4189, 1545-4479. doi: 10.1146/annurev-fluid-051820-020223. URL https://www.annualreviews.org/doi/10.1146/annurev-fluid-051820-020223.

J. Halcrow, J. F. Gibson, P. Cvitanović, and D. Viswanath. Heteroclinic connections in plane Couette flow. *Journal of Fluid Mechanics*, 621:365–376, February 2009. ISSN 0022-1120, 1469-7645. doi: 10.1017/S0022112008005065. URL https://www.cambridge.org/core/product/identifier/S0022112008005065/type/journal_article.

James M. Hamilton, John Kim, and Fabian Waleffe. Regeneration mechanisms of near-wall turbulence structures. *Journal of Fluid Mechanics*, 287:317–348, March 1995. ISSN 0022-1120, 1469-7645. doi: 10.1017/S0022112095000978. URL https://www.cambridge.org/core/product/identifier/S0022112095000978/type/journal_article.

C.Q Hoard, C.R Robertson, and A Acrivos. Experiments on the cellular structure in bénard convection. *International Journal of Heat and Mass Transfer*, 13(5):849–856, May 1970. ISSN 00179310. doi: 10.1016/0017-9310(70)90130-4. URL https://linkinghub.elsevier.com/retrieve/pii/0017931070901304.

B. Hof, P. G. J. Lucas, and T. Mullin. Flow state multiplicity in convection. *Physics of Fluids*, 11 (10):2815–2817, October 1999. ISSN 1070-6631, 1089-7666. doi: 10.1063/1.870178. URL https://pubs.aip.org/pof/article/11/10/2815/254396/Flow-state-multiplicity-in-convection.

Mohammad Z. Hossain, Chris D. Cantwell, and Spencer J. Sherwin. A spectral/ *hp* element method for thermal convection. *International Journal for Numerical Methods in Fluids*, 93(7):2380–2395, July 2021. ISSN 0271-2091, 1097-0363. doi: 10.1002/fld.4978. URL https://onlinelibrary.wiley.com/doi/10.1002/fld.4978.

Yuchou Hu, Robert E. Ecke, and Guenter Ahlers. Convection under rotation for Prandtl numbers near 1: Linear stability, wave-number selection, and pattern dynamics. *Physical Review E*, 55 (6):6928–6949, June 1997. ISSN 1063-651X, 1095-3787. doi: 10.1103/PhysRevE.55.6928. URL https://link.aps.org/doi/10.1103/PhysRevE.55.6928.

Harold Jeffreys. Some cases of instability in fluid motion. *Proceedings of the Royal Society of London. Series A, Containing Papers of a Mathematical and Physical Character*, 118(779):195–208, March 1928. ISSN 0950-1207, 2053-9150. doi: 10.1098/rspa.1928.0045. URL https://royalsocietypublishing.org/doi/10.1098/rspa.1928.0045.

Klavs F. Jensen, Erik O. Einset, and Dimitrios I. Fotiadis. Flow Phenomena in Chemical Vapor Deposition of Thin Films. *Annual Review of Fluid Mechanics*, 23(1):197–232, January 1991. ISSN 0066-4189, 1545-4479. doi: 10.1146/annurev.fl.23.010191.001213. URL https://www.annualreviews.org/doi/10.1146/annurev.fl.23.010191.001213.

J. John Soundar Jerome, Jean-Marc Chomaz, and Patrick Huerre. Transient growth in Rayleigh-Bénard-Poiseuille/Couette convection. *Physics of Fluids*, 24(4):044103, April 2012. ISSN 1070-6631, 1089-7666. doi: 10.1063/1.4704642. URL https://pubs.aip.org/pof/article/24/4/044103/257562/Transient-growth-in-Rayleigh-Benard-Poiseuille.

Yuki Kato and Kaoru Fujimura. Prediction of pattern selection due to an interaction between longitudinal rolls and transverse modes in a flow through a rectangular channel heated from below. *Physical Review E*, 62(1):601–611, July 2000. ISSN 1063-651X, 1095-3787. doi: 10.1103/PhysRevE.62.601. URL https://link.aps.org/doi/10.1103/PhysRevE.62.601.

Genta Kawahara and Shigeo Kida. Periodic motion embedded in plane Couette turbulence: regeneration cycle and burst. *Journal of Fluid Mechanics*, 449:291–300, December 2001. ISSN 0022-1120, 1469-7645. doi: 10.1017/S0022112001006243. URL https://www.cambridge.org/core/product/identifier/S0022112001006243/type/journal_article.

R.E. Kelly. The Onset and Development of Thermal Convection in Fully Developed Shear Flows. In *Advances in Applied Mechanics*, volume 31, pages 35–112. Elsevier, 1994. ISBN 978-0-12-002031-7. doi: 10.1016/S0065-2156(08)70255-2. URL https://linkinghub.elsevier.com/retrieve/pii/S0065215608702552.

K.J. Kennedy and A. Zebib. Combined free and forced convection between horizontal parallel planes: some case studies. *International Journal of Heat and Mass Transfer*, 26(3):471–474, March 1983. ISSN 00179310. doi: 10.1016/0017-9310(83)90052-2. URL https://linkinghub.elsevier.com/retrieve/pii/0017931083900522.

E.L. Koschmieder and S.G. Pallas. Heat transfer through a shallow, horizontal convecting fluid layer. *International Journal of Heat and Mass Transfer*, 17(9):991–1002, September 1974. ISSN 00179310. doi: 10.1016/0017-9310(74)90181-1. URL https://linkinghub.elsevier.com/retrieve/pii/0017931074901811.

P. Le Gal, A. Pocheau, and V. Croquette. Square versus Roll Pattern at Convective Threshold. *Physical Review Letters*, 54(23):2501–2504, June 1985. ISSN 0031-9007. doi: 10.1103/PhysRevLett.54.2501. URL https://link.aps.org/doi/10.1103/PhysRevLett.54.2501.

F.S. Lee and G.J. Hwang. The effect of asymmetric heating on the onset of thermal instability in the thermal entrance region of a parallel plate channel. *International Journal of Heat and Mass Transfer*, 34(9):2207–2218, September 1991. ISSN 00179310. doi: 10.1016/0017-9310(91)90047-I. URL https://linkinghub.elsevier.com/retrieve/pii/001793109190047I.

Dong-Jun Ma, De-Jun Sun, and Xie-Yuan Yin. Multiplicity of steady states in cylindrical Rayleigh-Bénard convection. *Physical Review E*, 74(3):037302, September 2006. ISSN 1539-3755, 1550-2376. doi: 10.1103/PhysRevE.74.037302. URL https://link.aps.org/doi/10.1103/PhysRevE.74.037302.

H. V. Mahaney, F. P. Incropera, and S. Ramadhyani. EFFECT OF WALL HEAT FLUX DISTRIBUTION ON LAMINAR MIXED CONVECTION IN THE ENTRANCE REGION OF A HORIZONTAL RECTANGULAR DUCT. *Numerical Heat Transfer*, 13(4):427–450, June 1988. ISSN 0149-5720. doi: 10.1080/10407788808913624. URL http://www.tandfonline.com/doi/abs/10.1080/10407788808913624.

Paul Manneville. Rayleigh-Bénard Convection: Thirty Years of Experimental, Theoretical, and Modeling Work. In Gerhard Höhler, Johann H. Kühn, Thomas Müller, Joachim Trümper, Andrei Ruckenstein, Peter Wölfle, Frank Steiner, Innocent Mutabazi, José Eduardo Wesfreid, and Etienne Guyon, editors, *Dynamics of Spatio-Temporal Cellular Structures*, volume 207, pages 41–65. Springer New York, New York, NY, 2006. ISBN 978-0-387-40098-3 978-0-387-25111-0. doi: 10.1007/978-0-387-25111-0_3. URL http://link.springer.com/10.1007/978-0-387-25111-0_3. Series Title: Springer Tracts in Modern Physics.

Á. Meseguer and L.N. Trefethen. Linearized pipe flow to Reynolds number 107. *Journal of Computational Physics*, 186(1):178–197, March 2003. ISSN 00219991. doi: 10.1016/S0021-9991(03)00029-9. URL https://linkinghub.elsevier.com/retrieve/pii/S0021999103000299.

H. W Müller, M Lücke, and M Kamps. Convective Patterns in Horizontal Flow. *Europhysics Letters (EPL)*, 10(5):451–456, November 1989. ISSN 0295-5075, 1286-4854. doi: 10.1209/0295-5075/10/5/011. URL https://iopscience.iop.org/article/10.1209/0295-5075/10/5/011.

H. W. Müller, M. Lücke, and M. Kamps. Transversal convection patterns in horizontal shear flow. *Physical Review A*, 45(6):3714–3726, March 1992. ISSN 1050-2947, 1094-1622. doi: 10.1103/PhysRevA.45.3714. URL https://link.aps.org/doi/10.1103/PhysRevA.45.3714.

M. Nagata. Three-dimensional finite-amplitude solutions in plane Couette flow: bifurcation from infinity. *Journal of Fluid Mechanics*, 217:519–527, August 1990. ISSN 0022-1120, 1469-7645. doi: 10.1017/S0022112090000829. URL https://www.cambridge.org/core/product/identifier/S0022112090000829/type/journal_article.

M. Nagata. Three-dimensional traveling-wave solutions in plane Couette flow. *Physical Review E*, 55(2):2023–2025, February 1997. ISSN 1063-651X, 1095-3787. doi: 10.1103/PhysRevE.55.2023. URL https://link.aps.org/doi/10.1103/PhysRevE.55.2023.

X. Nicolas, A. Mojtabi, and J. K. Platten. Two-dimensional numerical analysis of the Poiseuille–Bénard flow in a rectangular channel heated from below. *Physics of Fluids*, 9(2):337–348, February 1997. ISSN 1070-6631, 1089-7666. doi: 10.1063/1.869235. URL https://pubs.aip.org/pof/article/9/2/337/259822/Two-dimensional-numerical-analysis-of-the.

X. Nicolas, J.-M. Luijkx, and J.-K. Platten. Linear stability of mixed convection flows in horizontal rectangular channels of finite transversal extension heated from below. *International Journal of Heat and Mass Transfer*, 43(4):589–610, February 2000. ISSN 00179310. doi: 10.1016/S0017-9310(99)00099-X. URL https://linkinghub.elsevier.com/retrieve/pii/S001793109900099X.

Xavier Nicolas. Revue bibliographique sur les écoulements de Poiseuille–Rayleigh–Bénard : écoulements de convection mixte en conduites rectangulaires horizontales chauffées par le bas. *International Journal of Thermal Sciences*, 41(10):961–1016, October 2002. ISSN 12900729.

doi: 10.1016/S1290-0729(02)01374-1. URL https://linkinghub.elsevier.com/retrieve/pii/S1290072902013741.

Xavier Nicolas, Shihe Xin, and Noussaiba Zoueidi. Characterisation of a Wavy Convective Instability in Poiseuille-Rayleigh-Be´nard Flows: Linear Stability Analysis and Non Linear Numerical Simulations Under Random Excitations. In *2010 14th International Heat Transfer Conference, Volume 7*, pages 203–208, Washington, DC, USA, January 2010. ASMEDC. ISBN 978-0-7918-4942-2 978-0-7918-3879-2. doi: 10.1115/IHTC14-22256. URL https://asmedigitalcollection.asme.org/IHTC/proceedings/IHTC14/49422/203/360332.

C. Nonino and S. Del Giudice. Laminar mixed convection in the entrance region of horizontal rectangular ducts. *International Journal for Numerical Methods in Fluids*, 13(1):33–48, June 1991. ISSN 0271-2091, 1097-0363. doi: 10.1002/fld.1650130103. URL https://onlinelibrary.wiley.com/doi/10.1002/fld.1650130103.

William M'F. Orr. The Stability or Instability of the Steady Motions of a Perfect Liquid and of a Viscous Liquid. Part II: A Viscous Liquid. *Proceedings of the Royal Irish Academy. Section A: Mathematical and Physical Sciences*, 27:69–138, 1907. ISSN 00358975. URL http://www.jstor.org/stable/20490591. Publisher: Royal Irish Academy.

Steven A. Orszag. Accurate solution of the Orr–Sommerfeld stability equation. *Journal of Fluid Mechanics*, 50(4):689–703, December 1971. ISSN 0022-1120, 1469-7645. doi: 10.1017/S0022112071002842. URL https://www.cambridge.org/core/product/identifier/S0022112071002842/type/journal_article.

Hervé Pabiou, Sophie Mergui, and Christine Bénard. Wavy secondary instability of longitudinal rolls in RayleighPoiseuille flows. *Journal of Fluid Mechanics*, 542(-1):175, October 2005. ISSN 0022-1120, 1469-7645. doi: 10.1017/S0022112005006154. URL http://www.journals.cambridge.org/abstract_S0022112005006154.

Chaitanya S Paranjape. Onset of turbulence in plane Poiseuille flow. 2019. Publisher: IST Austria Klosterneuburg, Austria.

Chaitanya S. Paranjape, Yohann Duguet, and Björn Hof. Oblique stripe solutions of channel flow. *Journal of Fluid Mechanics*, 897:A7, August 2020. ISSN 0022-1120, 1469-7645. doi: 10.1017/jfm.2020.322. URL https://www.cambridge.org/core/product/identifier/S0022112020003225/type/journal_article.

Chaitanya S. Paranjape, Gökhan Yalnız, Yohann Duguet, Nazmi Burak Budanur, and Björn Hof. Direct Path from Turbulence to Time-Periodic Solutions. *Physical Review Letters*, 131(3):034002, July 2023. ISSN 0031-9007, 1079-7114. doi: 10.1103/PhysRevLett.131.034002. URL https://link.aps.org/doi/10.1103/PhysRevLett.131.034002.

M.R. Paul, K.-H. Chiam, M.C. Cross, P.F. Fischer, and H.S. Greenside. Pattern formation and dynamics in Rayleigh–Bénard convection: numerical simulations of experimentally realistic geometries. *Physica D: Nonlinear Phenomena*, 184(1-4):114–126, October 2003. ISSN 01672789. doi: 10.1016/S0167-2789(03)00216-1. URL https://linkinghub.elsevier.com/retrieve/pii/S0167278903002161.

Anne Pellew and Richard Vynne Southwell. On maintained convective motion in a fluid heated from below. *Proceedings of the Royal Society of London. Series A. Mathematical and Physical Sciences*, 176(966):312–343, November 1940. ISSN 0080-4630, 2053-9169. doi: 10.1098/rspa.1940.0092. URL https://royalsocietypublishing.org/doi/10.1098/rspa.1940.0092.

Sergio Pirozzoli, Matteo Bernardini, Roberto Verzicco, and Paolo Orlandi. Mixed convection in turbulent channels with unstable stratification. *Journal of Fluid Mechanics*, 821:482–516, June 2017. ISSN 0022-1120, 1469-7645. doi: 10.1017/jfm.2017.216. URL https://www.cambridge.org/core/product/identifier/S0022112017002166/type/journal_article.

Brendan B Plapp and Eberhard Bodenschatz. Core dynamics of multi-armed spirals in Rayleigh-Bénard convection. *Physica Scripta*, T67:111–116, January 1996. ISSN 0031-8949, 1402-4896. doi: 10.1088/0031-8949/1996/T67/022. URL https://iopscience.iop.org/article/10.1088/0031-8949/1996/T67/022.

Brendan B. Plapp, David A. Egolf, Eberhard Bodenschatz, and Werner Pesch. Dynamics and Selection of Giant Spirals in Rayleigh-Bénard Convection. *Physical Review Letters*, 81(24):5334–5337, December 1998. ISSN 0031-9007, 1079-7114. doi: 10.1103/PhysRevLett.81.5334. URL https://link.aps.org/doi/10.1103/PhysRevLett.81.5334.

Brendan Bryce Plapp. Spiral pattern formation in Rayleigh-Benard convection. *Ph.D. Thesis*, page 3118, December 1997. URL https://ui.adsabs.harvard.edu/abs/1997PhDT.......105P.

A. Prigent and O. Dauchot. "Barber pole turbulence" in large aspect ratio Taylor-Couette flow. *Physical Review Letters*, 89(1):014501, June 2002. ISSN 0031-9007, 1079-7114. doi: 10.1103/PhysRevLett.89.014501. URL http://arxiv.org/abs/cond-mat/0009241. arXiv:cond-mat/0009241.

Arnaud Prigent, Guillaume Grégoire, Hugues Chaté, and Olivier Dauchot. Long-wavelength modulation of turbulent shear flows. *Physica D: Nonlinear Phenomena*, 174(1-4):100–113, January 2003. ISSN 01672789. doi: 10.1016/S0167-2789(02)00685-1. URL https://linkinghub.elsevier.com/retrieve/pii/S0167278902006851.

Subhashis Ray and J. Srinivasan. Analysis of conjugate laminar mixed convection cooling in a shrouded array of electronic components. *International Journal of Heat and Mass Transfer*, 35(4):815–822, April 1992. ISSN 00179310. doi: 10.1016/0017-9310(92)90249-R. URL https://linkinghub.elsevier.com/retrieve/pii/001793109290249R.

Lord Rayleigh. LIX. *On convection currents in a horizontal layer of fluid, when the higher temperature is on the under side. The London, Edinburgh, and Dublin Philosophical Magazine and Journal of Science*, 32(192):529–546, December 1916. ISSN 1941-5982, 1941-5990. doi: 10.1080/14786441608635602. URL https://www.tandfonline.com/doi/full/10.1080/14786441608635602.

Satish C. Reddy and Dan S. Henningson. Energy growth in viscous channel flows. *Journal of Fluid Mechanics*, 252:209–238, July 1993. ISSN 0022-1120, 1469-7645. doi: 10.1017/S0022112093003738. URL https://www.cambridge.org/core/product/identifier/S0022112093003738/type/journal_article.

Satish C. Reddy, Peter J. Schmid, and Dan S. Henningson. Pseudospectra of the Orr–Sommerfeld Operator. *SIAM Journal on Applied Mathematics*, 53(1):15–47, February 1993. ISSN 0036-1399, 1095-712X. doi: 10.1137/0153002. URL http://epubs.siam.org/doi/10.1137/0153002.

Florian Reetz, Tobias Kreilos, and Tobias M. Schneider. Exact invariant solution reveals the origin of self-organized oblique turbulent-laminar stripes. *Nature Communications*, 10(1):2277, May 2019. ISSN 2041-1723. doi: 10.1038/s41467-019-10208-x. URL https://doi.org/10.1038/s41467-019-10208-x.

Osborne Reynolds. XXIX. An experimental investigation of the circumstances which determine whether the motion of water shall be direct or sinuous, and of the law of resistance in parallel channels. *Philosophical Transactions of the Royal Society of London*, 174:935–982, December 1883. ISSN 0261-0523, 2053-9223. doi: 10.1098/rstl.1883.0029. URL https://royalsocietypublishing.org/doi/10.1098/rstl.1883.0029.

Osborne Reynolds. IV. On the dynamical theory of incompressible viscous fluids and the determination of the criterion. *Philosophical Transactions of the Royal Society of London. (A.)*, 186:123–164, December 1895. ISSN 0264-3820, 2053-9231. doi: 10.1098/rsta.1895.0004. URL https://royalsocietypublishing.org/doi/10.1098/rsta.1895.0004.

H. T. Rossby. A study of Bénard convection with and without rotation. *Journal of Fluid Mechanics*, 36(2):309–335, April 1969. ISSN 0022-1120, 1469-7645. doi: 10.1017/S0022112069001674. URL https://www.cambridge.org/core/product/identifier/S0022112069001674/type/journal_article.

Sten Rüdiger and Fred Feudel. Pattern formation in Rayleigh-Bénard convection in a cylindrical container. *Physical Review E*, 62(4):4927–4931, October 2000. ISSN 1063-651X, 1095-3787. doi: 10.1103/PhysRevE.62.4927. URL https://link.aps.org/doi/10.1103/PhysRevE.62.4927.

A. Scagliarini, H. Einarsson, Á. Gylfason, and F. Toschi. Law of the wall in an unstably stratified turbulent channel flow. *Journal of Fluid Mechanics*, 781:R5, October 2015. ISSN 0022-1120, 1469-7645. doi: 10.1017/jfm.2015.498. URL https://www.cambridge.org/core/product/identifier/S002211201500498X/type/journal_article.

Andrea Scagliarini, Armann Gylfason, and Federico Toschi. Heat flux scaling in turbulent Rayleigh-Bénard convection with an imposed longitudinal wind. *Physical Review E*, 89(4):043012, April 2014. ISSN 1539-3755, 1550-2376. doi: 10.1103/PhysRevE.89.043012. URL http://arxiv.org/abs/1311.4598. arXiv:1311.4598 [physics].

H. Schlichting. Zur Enstehung der Turbulenz bei der Plattenströmung. *Nachrichten von der Gesellschaft der Wissenschaften zu Göttingen, Mathematisch-Physikalische Klasse*, 1933:181–208, 1933. URL http://eudml.org/doc/59420.

Hermann Schlichting and Klaus Gersten. Onset of Turbulence (Stability Theory). In *Boundary-Layer Theory*, pages 415–496. Springer Berlin Heidelberg, Berlin, Heidelberg, 2017. ISBN 978-3-662-52917-1 978-3-662-52919-5. doi: 10.1007/978-3-662-52919-5_15. URL http://link.springer.com/10.1007/978-3-662-52919-5_15.

A. Schlüter, D. Lortz, and F. Busse. On the stability of steady finite amplitude convection. *Journal of Fluid Mechanics*, 23(01):129, September 1965. ISSN 0022-1120, 1469-7645. doi: 10.1017/S0022112065001271. URL http://www.journals.cambridge.org/abstract_S0022112065001271.

Peter J. Schmid. Nonmodal Stability Theory. *Annual Review of Fluid Mechanics*, 39(1):129–162, January 2007. ISSN 0066-4189, 1545-4479. doi: 10.1146/annurev.fluid.38.050304.092139. URL https://www.annualreviews.org/doi/10.1146/annurev.fluid.38.050304.092139.

Peter J. Schmid and Dan S. Henningson. *Stability and Transition in Shear Flows*, volume 142 of *Applied Mathematical Sciences*. Springer New York, New York, NY, 2001. ISBN 978-1-4612-6564-1 978-1-4613-0185-1. doi: 10.1007/978-1-4613-0185-1. URL http://link.springer.com/10.1007/978-1-4613-0185-1.

Masaki Shimizu and Paul Manneville. Bifurcations to turbulence in transitional channel flow. *Physical Review Fluids*, 4(11):113903, November 2019. doi: 10.1103/PhysRevFluids.4.113903. URL https://link.aps.org/doi/10.1103/PhysRevFluids.4.113903. Publisher: American Physical Society.

Jennifer H. Siggers. Dynamics of target patterns in low-Prandtl-number convection. *Journal of Fluid Mechanics*, 475:357–375, January 2003. ISSN 0022-1120, 1469-7645. doi: 10.1017/S0022112002002896. URL https://www.cambridge.org/core/product/identifier/S0022112002002896/type/journal_article.

Arnold Sommerfeld. *Ein beitrag zur hydrodynamischen erklaerung der turbulenten fluessigkeitsbewegungen*. 1909.

Baofang Song, Dwight Barkley, Björn Hof, and Marc Avila. Speed and structure of turbulent fronts in pipe flow. *Journal of Fluid Mechanics*, 813:1045–1059, February 2017. ISSN 0022-1120, 1469-7645. doi: 10.1017/jfm.2017.14. URL https://www.cambridge.org/core/product/identifier/S0022112017000143/type/journal_article.

Herbert Brian Squire. On the stability for three-dimensional disturbances of viscous fluid flow between parallel walls. *Proceedings of the Royal Society of London. Series A, Containing Papers of a Mathematical and Physical Character*, 142(847):621–628, November 1933. ISSN 0950-1207, 2053-9150. doi: 10.1098/rspa.1933.0193. URL https://royalsocietypublishing.org/doi/10.1098/rspa.1933.0193.

J. J. Tao, Bruno Eckhardt, and X. M. Xiong. Extended localized structures and the onset of turbulence in channel flow. *Physical Review Fluids*, 3(1):011902, January 2018. doi: 10.1103/PhysRevFluids.3.011902. URL https://link.aps.org/doi/10.1103/PhysRevFluids.3.011902. Publisher: American Physical Society.

W. Tollmien. Über die Entstehung der Turbulenz. 1. Mitteilung. *Nachrichten von der Gesellschaft der Wissenschaften zu Göttingen, Mathematisch-Physikalische Klasse*, 1929:21–44, 1928. URL http://eudml.org/doc/59276.

Lloyd N. Trefethen. Pseudospectra of Linear Operators. *SIAM Review*, 39(3):383–406, January 1997. ISSN 0036-1445, 1095-7200. doi: 10.1137/S0036144595295284. URL http://epubs.siam.org/doi/10.1137/S0036144595295284.

Takahiro Tsukahara, Kaoru Iwamoto, Hiroshi Kawamura, and Tetsuaki Takeda. DNS of heat transfer in a transitional channel flow accompanied by a turbulent puff-like structure, September 2014a. URL http://arxiv.org/abs/1406.0586. arXiv:1406.0586 [physics].

Takahiro Tsukahara, Yasuo Kawaguchi, and Hiroshi Kawamura. An experimental study on turbulent-stripe structure in transitional channel flow, 2014b. URL https://arxiv.org/abs/1406.1378. Version Number: 2.

Takahiro Tsukahara, Yohji Seki, Hiroshi Kawamura, and Daisuke Tochio. DNS of turbulent channel flow at very low Reynolds numbers, September 2014c. URL http://arxiv.org/abs/1406.0248. arXiv:1406.0248 [physics].

Laurette S. Tuckerman and Dwight Barkley. Global Bifurcation to Traveling Waves in Axisymmetric Convection. *Physical Review Letters*, 61(4):408–411, July 1988. ISSN 0031-9007. doi: 10.1103/PhysRevLett.61.408. URL https://link.aps.org/doi/10.1103/PhysRevLett.61.408.

Laurette S Tuckerman and Dwight Barkley. Patterns and dynamics in transitional plane Couette flow. *Physics of Fluids*, 23(4), 2011. ISSN 1070-6631. Publisher: AIP Publishing.

Laurette S. Tuckerman, Tobias Kreilos, Hecke Schrobsdorff, Tobias M. Schneider, and John F. Gibson. Turbulent-laminar patterns in plane Poiseuille flow. *Physics of Fluids*, 26(11):114103, November 2014. ISSN 1070-6631, 1089-7666. doi: 10.1063/1.4900874. URL https://pubs.aip.org/pof/article/26/11/114103/315350/Turbulent-laminar-patterns-in-plane-Poiseuille.

Geoffrey K. Vallis, Douglas J. Parker, and Steven M. Tobias. A simple system for moist convection: the Rainy–Bénard model. *Journal of Fluid Mechanics*, 862:162–199, March 2019. ISSN 0022-1120, 1469-7645. doi: 10.1017/jfm.2018.954. URL https://www.cambridge.org/core/product/identifier/S0022112018009540/type/journal_article.

Milton Van Dyke and Milton Van Dyke. *An album of fluid motion*, volume 176. Parabolic Press Stanford, 1982.

D. Viswanath. Recurrent motions within plane Couette turbulence. *Journal of Fluid Mechanics*, 580: 339–358, June 2007. ISSN 0022-1120, 1469-7645. doi: 10.1017/S0022112007005459. URL https://www.cambridge.org/core/product/identifier/S0022112007005459/type/journal_article.

Fabian Waleffe. Exact coherent structures in channel flow. *Journal of Fluid Mechanics*, 435:93–102, May 2001. ISSN 0022-1120, 1469-7645. doi: 10.1017/S0022112001004189. URL https://www.cambridge.org/core/product/identifier/S0022112001004189/type/journal_article.

Fabian Waleffe. Homotopy of exact coherent structures in plane shear flows. *Physics of Fluids*, 15(6):1517–1534, June 2003. ISSN 1070-6631, 1089-7666. doi: 10.1063/1.1566753. URL https://pubs.aip.org/pof/article/15/6/1517/448391/Homotopy-of-exact-coherent-structures-in-plane.

José Eduardo Wesfreid. Henri Bénard: Thermal convection and vortex shedding. *Comptes Rendus. Mécanique*, 345(7):446–466, June 2017. ISSN 1873-7234. doi: 10.1016/j.crme.2017.06.006. URL https://comptes-rendus.academie-sciences.fr/mecanique/articles/10.1016/j.crme.2017.06.006/.

G. E. Willis and J. W. Deardorff. The oscillatory motions of Rayleigh convection. *Journal of Fluid Mechanics*, 44(04):661, December 1970. ISSN 0022-1120, 1469-7645. doi: 10.1017/S0022112070002070. URL http://www.journals.cambridge.org/abstract_S0022112070002070.

Xiangkai Xiao and Baofang Song. The growth mechanism of turbulent bands in channel flow at low Reynolds numbers. *Journal of Fluid Mechanics*, 883:R1, January 2020. ISSN 0022-1120, 1469-7645. doi: 10.1017/jfm.2019.899. URL https://www.cambridge.org/core/product/identifier/S0022112019008991/type/journal_article.

Shihe Xin, Xavier Nicolas, and Patrick Le Quéré. Stability analyses of Longitudinal Rolls of Poiseuille-Rayleigh-Bénard Flows in Air-Filled Channels of Finite Transversal Extension. *Numerical Heat Transfer, Part A: Applications*, 50(5):467–490, July 2006. ISSN 1040-7782, 1521-0634. doi: 10.1080/10407780600620079. URL http://www.tandfonline.com/doi/abs/10.1080/10407780600620079.

Xiangming Xiong, Jianjun Tao, Shiyi Chen, and Luca Brandt. Turbulent bands in plane-Poiseuille flow at moderate Reynolds numbers. *Physics of Fluids*, 27(4):041702, April 2015. ISSN 1070-6631, 1089-7666. doi: 10.1063/1.4917173. URL https://pubs.aip.org/pof/article/27/4/041702/1019208/Turbulent-bands-in-plane-Poiseuille-flow-at.